



Original article

3-Aryl-2-[1H-benzotriazol-1-yl]acrylonitriles: A novel class of potent tubulin inhibitors

Antonio Carta^{a,*}, Irene Briguglio^a, Sandra Piras^a, Giampiero Boatto^a, Paolo La Colla^b, Roberta Loddo^b, Manlio Tolomeo^c, Stefania Grimaudo^c, Antonietta Di Cristina^c, Rosaria Maria Pipitone^c, Erik Laurini^d, Maria Silvia Paneni^d, Paola Posocco^d, Maurizio Fermeglia^d, Sabrina Pricl^d

^a Dipartimento Scienze del Farmaco, Università degli Studi di Sassari, Via Muroni 23/a, 07100 Sassari, Italy

^b Dipartimento di Scienze e Tecnologie Biomediche, Sezione di Microbiologia e Virologia Generale e Biotecnologie Microbiche, Università degli Studi di Cagliari, Cittadella Universitaria, S.S. 554, Km 4,500, 09042 Monserrato, CA, Italy

^c Centro Interdipartimentale di Ricerca in Oncologia Clinica (C.I.R.O.C.), Università di Palermo, via del Vespro 129, 90127 Palermo, Italy

^d Molecular Simulation Engineering (MOSE) Laboratory, Department of Industrial Engineering and Information Technology (DI3), University of Trieste, Piazzale Europa 1, 34127 Trieste, Italy

ARTICLE INFO

Article history:

Received 20 March 2011

Received in revised form

10 June 2011

Accepted 11 June 2011

Available online 8 July 2011

Keywords:

3-Aryl-2-[1H-benzotriazol-1-yl]acrylonitriles

Antiproliferative activity

Tubulin

Homology studies

Molecular modeling study

Cell cycle distribution

Podophyllotoxin

Colchicine

ABSTRACT

During a screening for compounds that could act against *Mycobacterium tuberculosis*, a series of new cellular antiproliferative agents was identified. The most cytotoxic molecules were evaluated against a panel of human cell lines derived from hematological and solid human tumors. In particular, (*E*)-2-(1H-benzo[d][1,2,3]triazol-1-yl)-3-(4-methoxyphenyl)acrylonitrile (**1**) was found to be of a potency comparable to etoposide and greater than 6-mercaptopurine in all cell lines tested. Accordingly, a synthesis of a new series of (*E*)-2-(5,6-dichloro-1H-benzo[d][1,2,3]triazol-1-yl)-3-(4-R-phenyl)acrylonitriles was conducted in order to extend the studies of structure-activity relationship (SAR) for this class of molecules. With the aim to evaluate if 3-aryl-2-[1H-benzotriazol-1-yl]acrylonitriles were able to act like tubulin binding agents, the effects on cell cycle distribution of the most active compounds (**1**, **2a**, **3** and **4**) were analyzed in K562 cells. A detailed molecular modeling study of the putative binding mode of this series of compounds on tubulin is also reported.

© 2011 Elsevier Masson SAS. All rights reserved.

1. Introduction

Microtubules are cytoskeletal filaments that play a key role in the regulation of processes such as cell shape maintenance, segregation of chromosomes during mitosis, location of membrane-bound organelles, and transport. Structurally they resemble hollow cylinders in which the basic structural unit is constituted by an α , β -tubulin heterodimer. Both globular polypeptides (approximately 55 kDa each), are homologous but not identical, and combine stoichiometrically. Along the microtubule axis, tubulin dimers are joined to form protofilaments that associate laterally into a polar microtubule structure. By nature, these are structures characterized by highly dynamic behavior (e.g., fluctuations between phases of

elongation and shortening) and heavily involved in the process of cell mitosis. Indeed, at the onset of mitosis, cytoplasmic microtubules disassemble, and the free tubulin molecules rearrange to form the mitotic spindle, which bridges between the chromosomes in the center and the centrosomes at opposite poles of the cell. The spindle remains in dynamic equilibrium with the pool of free tubulin, and therefore must constantly add tubulin subunits to function properly [1]. Accordingly, any alteration of this dynamic equilibrium can induce cycle arrest and cell death (apoptosis) soon after.

Attacking the microtubule system is a common strategy employed in tumor cell proliferation inhibition; for this reason, the binding sites for compounds able to interfere with the microtubules/tubulin dynamics on tubulin are distinct and well characterized [2,3]. Accordingly, those molecules able to bind at the two natural compounds vinblastine and colchicine binding sites could inhibit tubulin assembly and are classified as microtubule destabilizing agents. In contrast, those compounds that bind to the

* Corresponding author. Tel.: +39 079 228722; fax: +39 079 228720.
E-mail address: acarta@uniss.it (A. Carta).

paclitaxel binding site prevent microtubule disassembly and are classified as microtubule stabilizing compounds [4].

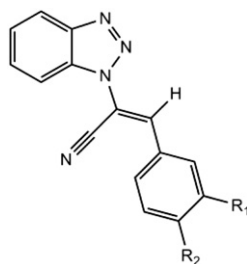
In the effort of developing new agents against *Mycobacterium strains*, our group found that some compounds belonging of the class of 3-aryl-1-benzotriazol-1-yl-acrylonitrile derivatives were active against the proliferation of a number of liquid and solid human tumors. The benzotriazole moiety characterizing this series of compounds has been amply studied by Katritzky et al. as a synthetic auxiliary, as it constitutes a good leaving group after reaction with a variety of carbonyl groups [5–7], whereas Sparatore et al. studied the biological properties [8,9] and described the interesting pharmacological activities of several benzotriazole derivatives bearing substituents at positions 1 or 2 [10–18]. Furthermore, some of us have developed a separate chemistry and investigated the biological potential of benzotriazoles [19–23]. In particular, we described several 3-aryl-2-benzotriazol-2-yl-acrylonitriles which were found endowed with antitubercular activity [24–27], partly retained by the corresponding amides and carboxylic acids [25]. In addition, we described 2-benzotriazol-(1)-yl-3-phenylacrylonitriles, which possess an interesting antiproliferative activity [26,27]. All these findings are summarized in Table 1, from which the promising activity in the nanomolar range of these compound series against both hematological and solid human tumors is evident.

On the basis of these results, (*E*)-2-(1*H*-benzo[*d*] [1,2,3]triazol-1-yl)-3-(4-methoxyphenyl)acrylonitrile **1** was identified as lead compound [26]. Interestingly, the benzotriazol-(1)-yl-3-phenylacrylonitrile derivative **1** bears no substituents at the benzene ring of the condensed heterocyclic moiety. In order to further potentiate its antiproliferative activity, several 5,6-dimethylbenzotriazol-(1)-yl-3-phenylacrylonitriles were synthesized in previous efforts, although with disappointing results [27].

In order to check whether the nature of the substituents on the benzene ring could act favorably toward the biological activity of these molecules, we then synthesized the new series of (*E*)-2-(5,6-dichloro-1*H*-benzo[*d*] [1,2,3]triazol-1-yl)-3-(4-*R*-phenyl)acrylonitriles **1a–3a** depicted in Fig. 1. The substituents on the phenyl-moiety (indicated with *R* in Fig. 1) have been selected among those showing the best antiproliferative activity in the previous series. All new derivatives have been evaluated for cytotoxicity against MT-4 cells and for their antiproliferative activity against a panel of cell lines derived from hematological and solid human tumors.

With the aim of understanding the mechanism of action of this class of antiproliferative agents, at the beginning we performed an extensive analysis of the scientific literature to detect possible structural analogies with other molecules endowed with similar antiproliferative activity. Partial similarities were found with many molecules, but the most compelling were those with derivatives of resveratrol and trimethoxy-aryl-thiophene, well-known antimetabolic agents acting binding at the colchicine-binding site of tubulin [28]. Recent studies conducted by other groups on these derivatives have confirmed their ability to inhibit the polymerization of tubulin thereby preventing the formation of spindle cells by blocking cell replication in its metaphase [29–31]. Further, these experimental pathways have been paralleled and assisted by molecular modeling investigations, aiming both at optimizing the synthetic strategy and efforts, and at exploring the eventual molecular interactions between antimetabolic inhibitors and tubulin. Therefore, we decided to attempt to develop a structure-activity relationship (SAR) for all these compound sets by means of molecular modeling ansatz based on a hierarchical procedure consisting of i) three-dimensional pharmacophore development for the compound series, ii) docking studies guided by the pharmacophore requirements, and

Table 1
Antiproliferative activity against hematological and solid human tumor-derived cell lines of (*E*)-2-(1*H*-benzo[*d*] [1,2,3]triazol-1-yl)-3-(3-*R*₁-4-*R*₂-phenyl)acrylonitriles **1–4**.



Compd	R ₁	R ₂	^a CC ₅₀ MT-4	^b CC ₅₀							
				^c CCR FCCM	^d WIL2 NS	^e CCR FSB	^f SKM EL28	^g MCF7	^h SKM ES1	ⁱ HepG2	^j DU145
1	H	OCH ₃	0.05	0.2	0.1	0.09	0.2	0.1	0.6	0.8	0.6
2	H	CH ₃	0.5	0.2	0.2	0.07	0.3	0.7	1.7	2.2	0.5
3	H	Br	0.4	0.4	0.6	0.3	1.1	0.7	2.4	2.1	1.7
4		O-CH ₂ -O	0.1	0.9	0.6	0.6	3.3	1.3	3.3	3.1	3.4
6MP			0.1	1.0	3.0	1.1	15	3.2	58.0	8.0	2.0
Etoposide			0.09	0.09	0.2	0.1	1.2	1.0	0.3	0.7	0.4

^a Compound concentration (μM) required to reduce the viability of mock-infected MT-4 cells by 50%, as determined by the MTT method. Data represent mean values for two separate experiments. Variation among duplicate samples was less than 15%.

^b Compound concentration (μM) required to reduce cell proliferation by 50%, as determined by the MTT method, under conditions allowing untreated controls to undergo at least three consecutive rounds of multiplication. Data represent mean values for two separate experiments. Variation among duplicate samples was less than 15%.

^c CD4⁺ human acute T-lymphoblastic leukemia.

^d Human splenic B-lymphoblastoid cells.

^e Human acute B-lymphoblastic leukemia.

^f Human skin melanoma.

^g Human breast adenocarcinoma.

^h Human lung squamous carcinoma.

ⁱ Human hepatocellular carcinoma.

^j Human prostate carcinoma.

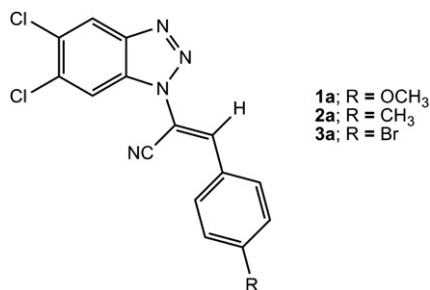
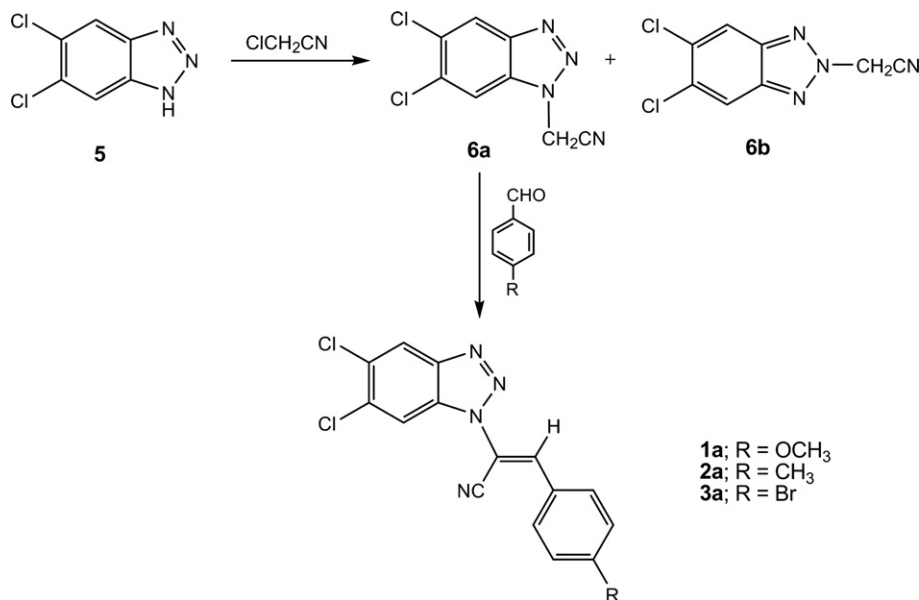


Fig. 1. Structure of the (*E*)-2-(5,6-dichloro-1*H*-benzo[*d*] [1,2,3]triazol-1-yl)-3-(4-*R*-phenyl)acrylonitrile derivatives considered in this work.

iii) estimation of the affinity of each compound toward tubulin by means of atomistic molecular dynamics simulations. According to this computational recipe, a putative binding mode of our series of compounds onto tubulin was obtained, and the structural bases of the biological results discussed above were investigated in details.

2. Chemistry

The intermediate compound 2-(5,6-dichloro-1*H*-benzo[*d*] [1,2,3]triazol-1-yl)acetonitrile **6a** was prepared as described in Scheme 1 by condensation of 5,6-dichloro-1*H*-benzo[*d*] [1,2,3]triazole **5** with chloroacetonitrile in dimethylformamide (DMF) in the presence of triethylamine (Et₃N). Compound **5** was in turn prepared following a procedure previously reported [32]. The synthesis of the new series of (*E*)-2-(5,6-dichloro-1*H*-benzo[*d*] [1,2,3]triazol-1-yl)-3-(4-*R*-phenyl)acrylonitriles **1a–3a** was accomplished by a straightforward condensation of **6a** with the appropriate commercially available aldehydes, following the procedure early described for **1** [26]. In this new series, among the two possible geometric isomers (*E*/*Z*), *E*-isomers were obtained as the sole product. Spectral (IR, UV–vis, ¹H NMR) and analytical (elemental analyses, MS) data obtained for all new compounds are in accordance with those of the previously described counterparts [26], and support the assigned chemical structure.



Scheme 1. Synthetic route to (*E*)-2-(5,6-dichloro-1*H*-benzo[*d*] [1,2,3]triazol-1-yl)-3-(4-*R*-phenyl)acrylonitrile derivatives **1a–3a**.

3. Microbiology

All new compounds were evaluated for cytotoxicity toward MT-4 cells and for antiproliferative activity against a panel of human cell lines derived from hematological (CCRF-CEM, WIL-2NS and CCRFSB) and solid (SKMEL28, MCF7, SKMES-1, HepG2, and DU145) human tumors. The same antitumor agents previously used, 6-mercapto-purine (6 MP) and etoposide (a semisynthetic derivative of podophyllotoxin [33]) were tested as reference drugs.

4. Cell cycle analysis

Because molecules exhibiting activity on tubulin should cause the alteration of cell cycle parameters leading to a preferential G2/M blockade, the effects of the most active compound of the new series (**2a**) on cell cycle distribution were analyzed in K562 cells. The relevant data were then compared to those obtained with the non-halogenated compounds **1**, **3** and **4**. Cells were exposed to each compound used at the TGI (total growth inhibition concentration), and after 24 h cell cycle analysis was performed as described in materials and methods. As expected from the results shown in Fig. 2, compound **2a** induced a marked increase of the G2-M peak (67% vs. 18% of the non-treated control), consistent with its tubulin binding activity. As shown in Fig. 2, compounds **1** and **4** also act on the G2/M phase of the cell cycle (70.5% and 66.34%, respectively), while compound **3** caused an increase of both G0-G1 and G2-M peaks, suggesting that its cell growth inhibition activity could be only partially correlated to its tubulin binding activity.

5. [³H]Colchicine competition binding assay

To further confirm the tubulin binding activity of the title compounds, we assessed their capability to compete with colchicine or paclitaxel for binding to tubulin by resorting to a competitive scintillation proximity assay [34] using compound **4** as reference. As shown in Fig. 3, we found that compound **4** competitively inhibited [³H]colchicine binding to biotinylated tubulin with an IC₅₀ value of 0.85 μM whereas the corresponding value for colchicine was 1.02 μM. At the same time, compound **4** did not compete with [³H]paclitaxel. No stabilization of the colchicine

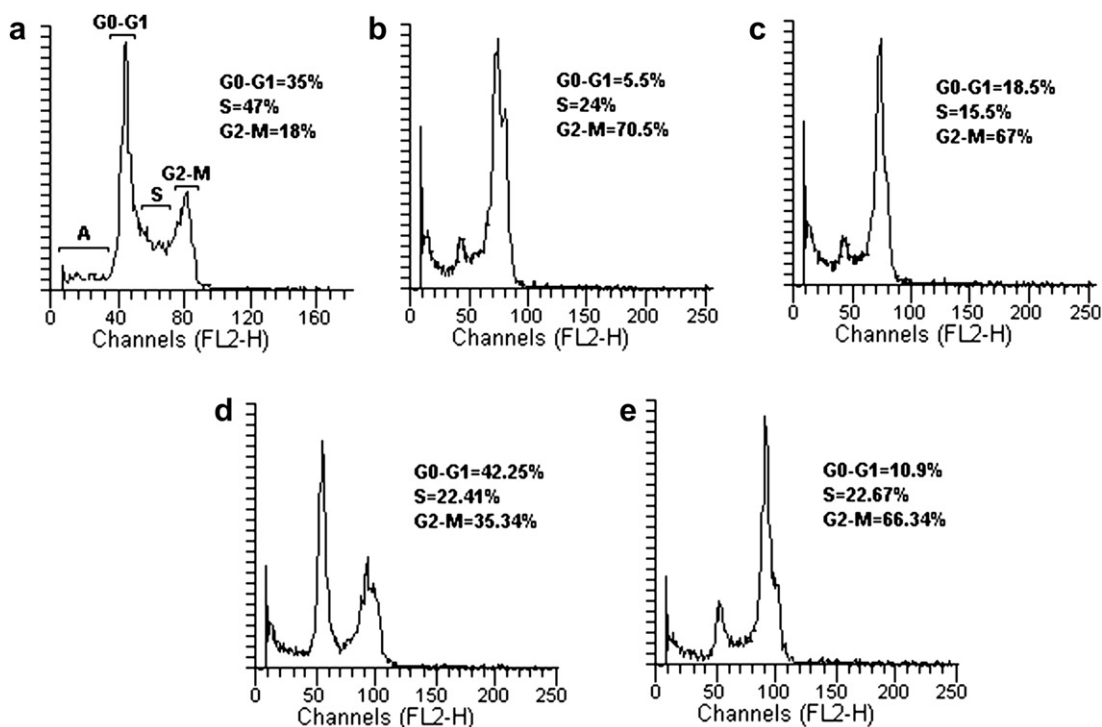


Fig. 2. Effects of compounds **1** (panel **b**), **2a** (panel **c**), **3** (panel **d**), and **4** (panel **e**) on DNA content/cell following the treatment of K562 cells for 24 h. The cells were cultured without any compounds (panel **a**) or with each compound used at TGI (total growth inhibition concentration). Cell cycle distribution was analyzed by the standard propidium iodide procedure, as described in Material and Methods. Sub-G0-G1 (A), G0-G1, S, and G2-M cells are indicated in panel **a**.

binding was observed, as it is found for Vinca site binders [35,36]. We could then conclude that binding to tubulin at the colchicine binding site for compound **4** and all other compounds of this series is highly probable. Accordingly, the capacity to interact with the mitotic spindle contributes to the antiproliferative activity of these compounds.

6. Molecular modeling

6.1. Three-dimensional pharmacophore model generation

A prerequisite for the development of a three-dimensional (3D) pharmacophore model for tubulin inhibitors is the correlation of a characteristic and reproducible biological activity to the structural information of the respective compound. As biological activity,

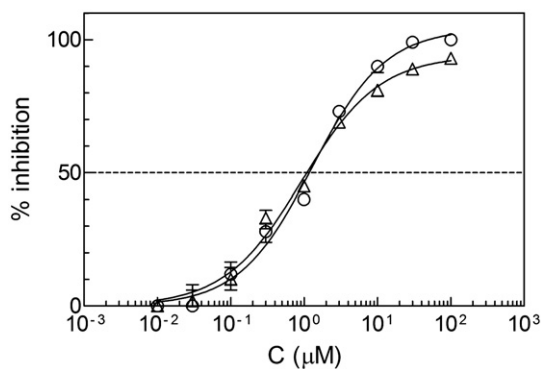


Fig. 3. [³H]Colchicine competition binding assay of compound **4** and colchicine. Radio labeled colchicine, unlabeled compound, and biotin-labeled tubulin were incubated together at 37 °C for 2 h. Symbols legend: ○, colchicine; △, **4**.

a variety of parameters such as IC₅₀, EC₅₀ or CC₅₀ values, binding/inhibition constant, or even uptake rates may be used. Because our interest was primarily the study of high-affinity inhibitors of tubulin in order to prevent cancer cell proliferation, we decided to use the CC₅₀ values of our compounds against MT-4 cells as the biological parameter to develop the pharmacophore model. To obtain a realistic 3D quantitative-structure activity relationship (QSAR) adequately describing the interactions between a ligand series and their target with a high predictability, however, several aspects have to be considered. Firstly, a collection of minimum 15 chemically diverse compounds is necessary to constitute the so-called training set; also, the biological activity of the training set compounds should cover at least 4 orders of magnitude to avoid model biasing. Thus, to enrich the compound sets listed in Tables 1 and 2 of the present paper, for the generation of the 3D pharmacophore model we also considered three series of previously synthesized compounds tested for activity as tubulin inhibitors using the same methodology employed in the present work [24–27]. These compounds are shown in Table 3, together with their biological data.

A three-dimensional pharmacophore model captures the three-dimensional arrangement of the structural features shared by all active molecules that are presumably essential for the desired pharmacological activity. The *HypoGen* algorithm of *Discovery Studio (DS) Catalyst* [37] allows a maximum of five features to be present in the pharmacophore generation process. Preliminary runs including, among others, the negative charge (NC) site, the positive ionizable (PI), the hydrogen bond acceptor lipid (HBAI), and the hydrophobic aliphatic (HYAI), confirmed that these features were never used in the generation of the pharmacophore models. Thus, all these features were removed from the list. In summary, the following five chemical features were taken into account for hypothesis generation with *HypoGen*: hydrogen

Table 2
Cytotoxicity and antiproliferative activity against hematological and solid human tumor-derived cell lines of compounds **1a–3a**.

Compd	^a CC ₅₀	^b CC ₅₀							
	MT-4	^c CCRF CEM	^d WIL2 NS	^e CCR FSB	^f SKM EL28	^g MCF7	^h SKM ES1	ⁱ HepG2	^j DU145
1a	14	>100	>100	>100	>100	>100	>100	>100	>100
2a	1.7	2.8	7.0	2.8	20	27	27	21	17
3a	5.4	5.3	18	12	10	8.4	10	12	7
6MP	0.1	1.0	3.0	1.1	15	3.2	58.0	8.0	2.0
Etoposide	0.09	0.09	0.2	0.1	1.2	1.0	0.3	0.7	0.4

^a Compound concentration (μM) required to reduce the viability of mock-infected MT-4 cells by 50%, as determined by the MTT method. Data represent mean values for two separate experiments. Variation among duplicate samples was less than 15%.

^b Compound concentration (μM) required to reduce cell proliferation by 50%, as determined by the MTT method, under conditions allowing untreated controls to undergo at least three consecutive rounds of multiplication. Data represent mean values for two separate experiments. Variation among duplicate samples was less than 15%.

^c CD4⁺ human acute T-lymphoblastic leukemia.

^d Human splenic B-lymphoblastoid cells.

^e Human acute B-lymphoblastic leukemia.

^f Human skin melanoma.

^g Human breast adenocarcinoma.

^h Human lung.

ⁱ Human hepatocellular carcinoma.

^j Human prostate carcinoma.

bond acceptor (HBA), hydrogen bond donor (HBD), hydrophobic aromatic (HYAr), ring aromatic (RA) and more generic hydrophobic feature (HY).

A total of 10 hypotheses were generated by the *HypoGen* algorithm, all characterized by the same three features: HBA, HYAr, and Ar. The total hypothesis cost of these ten best models varies between 100.1 for the best ranked model (Hypo1) to 108.4 for the lowest ranked one (Hypo10), as shown in Table 4. Such a confined difference (8.6 bits) reflects both the homogeneity of the generated hypotheses and the adequacy of the molecular training set. The difference between the null and the fixed costs, which should be higher than 70 to guarantee a robust correlation, is 104.2 in our case. This corresponds to a chance of true correlation in the data greater than 90% [38]. Further, the evidence that for all hypotheses the total costs are sensibly closer to the fixed cost (109.7) than to the null cost (212.1) also constitutes an indication that meaningful models are obtained. As reported in Table 4, for Hypo1 the configurational cost value is equal to 11.6, which is well below the threshold value of 17. Finally, the root-mean-square deviations (RMSD) and the correlation coefficients (ρ) between estimated and experimental affinities range from 1.6 to 1.9, and from 0.83 to 0.88, respectively. Considering that all the generated pharmacophores map the molecules of the training set in a similar way, the first model (Hypo1), characterized by the highest cost difference, the lowest RMSD, and the best ρ values was selected for further analysis.

The affinities of 25 compounds in the training set estimated using Hypo1 are reported in Table 5, along with the experimental values and the relevant errors (expressed as the ratio between estimated and experimental values). This Table clearly shows that all activities are well predicted, all errors being mostly below 3.6. Fig. 4 shows the mapping of compounds **1**, **33**, and **36** onto Hypo1, respectively. As can be seen from Fig. 4(A), in **1** the aromatic ring of the benzotriazole moiety matches the HYAr feature, whilst the cyano group and one nitrogen atom of the triazole ring nicely map the two HBD functions, respectively. The phenyl group bearing the $-\text{OCH}_3$ substituent finally overlaps the RA feature of the pharmacophore. The estimated activity for **1** is 0.13 μM , while the corresponding experimental CC₅₀ is 0.05 μM . Fig. 4(B) is an example of a pharmacophore mapping of a compound that is less active than the former one. Compound **36** does not map all the features encoded in Hypo1. In fact, **36** maps the HYAr function, again by means of the benzomoiety of the heterocycle; however, it does not map one of the HBD feature, and the mapping of the remaining RA is not perfect. According to this partial mapping, this compound is

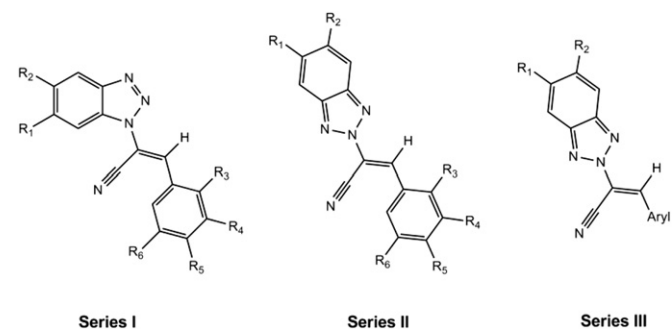
predicted to be quite less active (estimated CC₅₀ = 445 μM , experimental CC₅₀ = 375 μM). Finally, Fig. 4(C) depicts **33**, the least active compound, mapped onto Hypo1. As can be seen from this panel, the molecule **33** fails to map one of the HBD features and the HYAr function. The remaining HBD is mapped again by the cyano group and the RA is overlaid by the phenyl ring of the aromatic ring of the benzotriazole. This poor mapping scheme fully accounts for the very low activity of this compound (estimated CC₅₀ = 42,800 μM , experimental CC₅₀ = 20,000 μM).

To check further on the usefulness of the generated 3D pharmacophore, we validated the model by mapping a test set of 11 compounds (see Tables 3 and 6). Indeed, a good correlation coefficient (0.84) was observed when a regression analysis was performed by mapping the test set onto the features of the best pharmacophore hypothesis Hypo1. The predicted and the experimental CC₅₀ values for the test set along with the respective errors are given in Table 6. The average error in predicting the affinity of the test set molecules is 1.4; therefore, given the inherent simplicity of the pharmacophoric approach, and considering the intrinsic variability of the biological responses, we can conclude that the ability of the present 3D pharmacophore model in predicting the activity of these molecular series as tubulin inhibitor is satisfactory. Fig. 5 shows the mapping of one test set molecule **14** to Hypo1.

A second test was performed to verify the statistical significance of 3D pharmacophore model Hypo1, based on a randomization procedure derived from the Fisher method [39] available in the *DS Catalyst* suite of programs. According to the validation procedure, the experimental affinities of the compounds in the training set were scrambled randomly, and the resulting new training set was used for a new *HypoGen* run. The parameters used in running these calculations were the same employed in the initial *HypoGen* calculations and, since a 99% confidence level was selected, 99 random hypothesis runs were performed. The resulting data clearly indicate that all values generated after randomization produced hypotheses with no predictive values. Indeed, none of the outcome hypotheses had lower cost score, better correlation or smaller root-mean-square deviation than the initial one. Table 7 lists the first 10 lowest total score values of the resulting 99 hypotheses for our test set molecules. In conclusion, there is a 99% chance for the best hypothesis to represent a true correlation in the training set affinity data for the present classes of compounds.

As a last statistical test, the *leave-one-out method*, which consists of re-computing the hypothesis by excluding from the training set one molecule at a time, was performed. Basically, this test aims at

Table 3
Additional set of molecules used in the training set and test set for 3D pharmacophore model generation.



Compd	R ₁	R ₂	R ₃	R ₄	R ₅	R ₆	CC ₅₀ ^a
Series I							
7	H	H	H	O–CH ₂ –O		H	0.1
8	H	H	H	H	Cl	H	0.4
9	H	H	H	NO ₂	H	H	0.4
10	CH ₃	CH ₃	H	NO ₂	H	H	0.5
11	H	CF ₃	H	NO ₂	H	H	0.7
12	CH ₃	CH ₃	H	O–CH ₂ –O		H	1.3
13	H	H	H	OCH ₃	OCH ₃	OCH ₃	2.5
14	H	H	H	H	H	H	4.0
15	H	H	H	OCH ₃	H	H	4.7
16	H	H	Cl	H	Cl	H	6.0
17	H	H	H	OCH ₃	OCH ₃	H	7.5
18	H	H	OCH ₃	H	H	H	8.3
19	H	H	H	H	COOH	H	17
20	CH ₃	CH ₃	H	H	Cl	H	24
21	H	H	I	H	H	H	25
22	H	H	NO ₂	H	H	H	31
23	CF ₃	H	H	O–CH ₂ –O		H	52
24	CF ₃	H	H	H	OCH ₃	H	200
Series II							
25	H	H	H	H	NO ₂	H	0.4
26	H	H	H	H	H	H	12
27	H	H	H	H	Cl	H	16
28	H	H	H	H	COOH	H	16
29	H	H	H	H	CH ₃	H	20
30	H	H	H	H	F	H	32
31	H	H	H	OCH ₃	OCH ₃	H	360
32	H	H	H	OCH ₃	OCH ₃	OCH ₃	7500
33	H	H	H	O–CH ₂ –O		H	20000
34	CH ₃	CH ₃	H	OCH ₃	OCH ₃	H	12000
Compd	R ₁	R ₂	ARYL			CC ₅₀ ^a	
Series III							
35	H	H				132	
36	H	H				375	
37	H	H				5000	
38	H	H				10000	

^a Compound concentration (μM) required to reduce the viability of mock-infected MT-4 cells by 50%, as determined by the MTT method.

verifying whether the correlation is strongly dependent on one particular compound in the training set. The test is positive if the affinity of each excluded molecule is correctly predicted by the corresponding one-missing hypothesis. For each of the 23 new

Table 4
Composition, ranking score, statistical parameters, and cost analysis (expressed in bits) of the top 10 generated hypotheses.

Hypothesis	Total cost	ΔCost ^a	RMDS	ρ
1	138.4	73.7	1.64	0.876
2	140.1	72.0	1.74	0.859
3	140.8	71.3	1.75	0.857
4	141.6	70.5	1.71	0.846
5	142.0	70.1	1.79	0.851
6	143.8	68.3	1.83	0.843
7	144.0	68.1	1.82	0.845
8	146.0	66.1	1.86	0.839
9	146.7	65.4	1.87	0.837
10	147.0	65.1	1.91	0.828

^a ΔCost = Cost difference = null cost–total cost. Null cost: 212.1. Fixed cost: 107.9. Configurational cost: 11.6.

hypotheses generated according to this method we did not obtained meaningful differences between Hypo1 and each hypothesis resulting from the exclusion of one compound at a time, in terms of correlation coefficients, feature composition of the pharmacophore, and quality of the predicted affinity of the excluded molecule.

According to all evidences highlighted above, we believe that our *in silico* 3D pharmacophore model accounts for tubulin inhibitory activity of our set of compounds and, despite its inherent simplicity, its predictive power is quite robust and can then be employed as a guide for discovering a possible binding site and for the successive docking of the inhibitors focus of the present study within on their putative binding site on human tubulin.

6.2. Docking and calculations of binding free energy by MM/PBSA method

Docking studies were carried out to obtain putative binding modes of our series of compounds to tubulin, and to investigate the structural basis of the biological results discussed above. In the absence of any information about the docking modes for our

Table 5
Experimental and estimated activity values (CC₅₀) of the training set compounds used to develop pharmacophore hypothesis for tubulin inhibitors.

Compd	CC ₅₀ (μM)			
	Experimental	Estimated	Mapping	Error ^a
1	0.05	0.13	1 1 1 1	2.6
7	0.1	0.38	1 1 1 1	3.8
8	0.4	0.58	1 1 1 1	1.5
11	0.7	1.1	1 1 1 1	1.6
12	1.3	1.6	1 1 1 1	1.2
13	2.5	2.3	1 1 1 1	–1.1
15	4.7	2.1	1 1 1 1	–2.2
16	6.0	9.9	1 1 * 1	1.7
17	7.5	2.1	1 1 1 1	–3.6
18	8.3	13	1 1 1 1	1.6
20	24	19	1 1 * 1	–1.3
22	31	56	1 * 1 1	1.8
24	200	258	1 1 1 1	–3.4
26	12	8.0	1 1 1 1	–1.5
29	20	33	1 * 1 1	1.7
31	360	920	1 * * 1	2.6
32	7500	9100	1 1 * 1	1.2
33	20000	42800	1 * * 1	2.1
35	132	99	1 * 1 1	7.5
36	375	445	1 * 1 1	1.2
37	5000	1400	1 * * 1	–3.6
38	10000	6700	1 * * 1	–1.5
1a	14	18	1 1 1 1	1.3
2a	1.7	2.7	1 * 1 1	1.6
3a	5.4	4.8	1 1 1 1	–1.1

^a Values in the error column represent the ratio of the estimated to experimental affinity, or its negative inverse if the ratio is less than one.

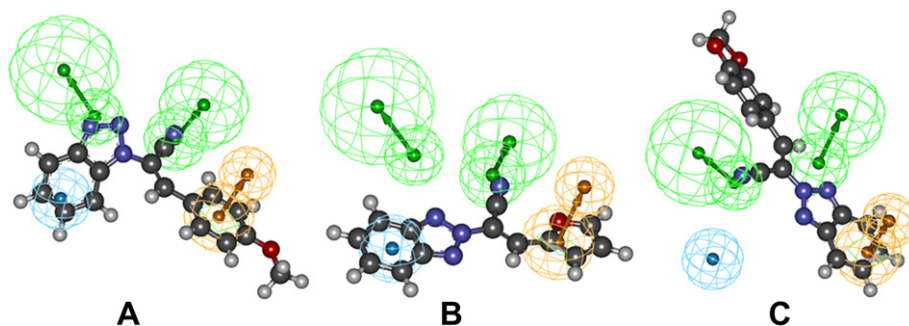


Fig. 4. Pharmacophore mapping of compound **1** (A), **36** (B), and **33** (C) in the training set. The hypothesis features are portrayed as meshed spheres, color-coded as follows: light green, HBA; light blue, HYAr; light orange, RA. HBA is actually represented as a pair of spheres, the smaller sphere representing the location of the HBA atom on the ligand and the larger one the location of an HB donor on the receptor. Compounds are depicted as atom-colored sticks-and-balls: carbon, dark gray; oxygen, red; nitrogen, blue, hydrogen, white. (For interpretation of the references to colour in this figure legend, the reader is referred to the web version of this article.)

molecules, we decided to apply some blank tests to verify the reliability of the overall computational procedure adopted. Accordingly, we began by modeling, docking and calculating the free energy of binding (and the corresponding IC_{50} values) for podophyllotoxin and colchicine to human β -tubulin. The best docked structures for both podophyllotoxin and colchicine, i.e., the configurations with lowest docking energy in each prevailing cluster, were then compared with the corresponding crystal structures and subjected to MM/PBSA calculations [40] to obtain the free energy of binding and, hence, the corresponding IC_{50} value [41,42].

Fig. 6 shows a superposition between the co-crystallized conformations of podophyllotoxin and colchicine into the allosteric binding site of tubulin, and the corresponding docked conformations obtained upon application of the computational strategy adopted in this work. As it can be seen, the agreement between crystal and docked structures is excellent: the root-mean-square deviation (RMSD) between the docked configurations and the relevant crystal structures of these test molecules is equal to 0.5 Å and 0.3 Å, respectively.

To further test whether our computational recipe was feasible to predict unknown ligand binding modes to tubulin, we decided to apply it to MDL 27048 ([trans-1-(2,5-dimethoxyphenyl)-3-[4-(dimethylamino)phenyl]-2-methyl-2-propen-1-one]), and CHALC101, two structurally different but potent destabilizers of microtubule formation for which only biological data and/or modeling speculations are available [43,44]. As depicted in Fig. 7, MDL 27048 and CHALC101 are found to share the same binding site of podophyllotoxin and colchicine, in harmony with previous modeling results [44], the overlapping of the binding site accounting for the experimentally verified competition among colchicine, podophyllotoxin, MDL 27048 and CHALC101 in tubulin binding.

Table 6

Experimental and estimated activity values of the test set compounds used to develop pharmacophore hypothesis for tubulin inhibitors.

CC ₅₀ (μM)			
Compd	Experimental	Estimated	Error ^a
9	0.4	0.8	2.0
10	0.5	1.8	3.6
14	4	10	2.5
19	17	4	-4.3
21	25	14	-1.8
23	52	76	1.5
25	0.4	0.1	-4.0
27	16	10	-1.6
28	16	23	1.4
30	32	35	1.1
34	12000	22000	1.8

^a Values in the error column represent the ratio of the estimated to experimental affinity, or its negative inverse if the ratio is less than one.

In the light of these blank-test results, and of the fact that a similar computational ansatz was already successfully applied by our group to estimate the activity of other protein inhibitors for which no structural information were available [44–47], the conceived modeling/docking procedure was applied for predicting the binding mode of the present series of compounds in the tubulin binding site targeted by podophyllotoxin and colchicine.

Twenty nanoseconds molecular dynamics simulations were then performed on colchicine and podophyllotoxin in complex with tubulin. Overall, compared to the corresponding crystal structures, the RMSDs of the ligands and the protein backbone are about 0.5 and 0.8 Å, respectively. The same protocol was applied to MDL 27048, CHAL101, and a subset of our title compounds. Fig. 8 shows an equilibrated snapshot of compound 1/tubulin complex as an example. From this figure it is evident how compound 1 interacts extensively with β -tubulin mainly via van der Waals contacts (coherently with previous modeling evidences reported for podophyllotoxin [48]), while only two residues (i.e., Ala α 180 and Val α 181) of α -tubulin are engaged in hydrophobic interactions with the inhibitor. More importantly, the predicted binding mode is found to comply with the pharmacophore hypothesis requirements (see Fig. 4A). In fact, the first hydrogen bond acceptor (HBA) feature on the inhibitor, represented by the triazole N₃, localizes hydrogen bond acceptor structures that are in an ideal position for forming a stabilizing hydrogen bond (average dynamic distances \leq 2.8 Å) with the donor guanidinium group of Lys β 350 on the receptor. The benzotriazole moiety is embedded in a hydrophobic pocket consisting of the side chains of Lys β 252, Leu β 253, Asn β 256,

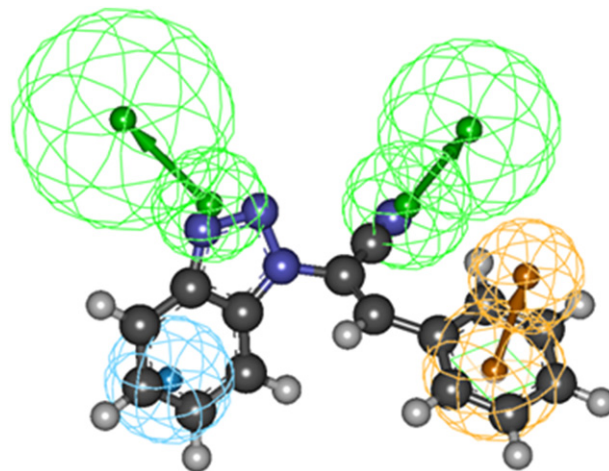


Fig. 5. Pharmacophore mapping of compound **14** in the test set. Hypothesis features are color-coded as in Fig. 3.

Table 7

Output parameters of the 10 lowest cost hypotheses resulting from the statistical evaluation according to the Fisher method validation procedure for the tubulin inhibitors.

Hypothesis	ρ	RMDS	Total cost
1	0.816	1.689	140.0
2	0.802	1.711	152.1
3	0.789	1.745	154.4
4	0.782	1.796	155.4
5	0.769	1.802	155.8
Hypo1	0.876	1.644	138.4
6	0.745	1.834	158.1
7	0.743	1.871	159.8
8	0.740	1.992	160.0
9	0.737	2.014	160.4
10	0.728	2.109	160.8

Met β 257, Thr β 312, Ala β 314, Lys β 350, which all concur to satisfy the hydrophobic aromatic feature (HYAr) of the 3D pharmacophore. The *p*-methoxyphenyl ring fits in a pocket lined by residues Ile β 236, Ser β 239, Leu β 240, Leu β 246, Ala β 248, Leu β 253, the cyano N atom being located within hydrogen bond distance (average dynamic length (ADL) = 3.2 Å) of the hydroxyl group of Thr β 312, as required by the second HBA feature of the pharmacophore. The C=C bond is stabilized by favorable hydrophobic interactions due to the vicinity of the side chains of Leu β 253 and Ile β 236, whilst the phenyl group bearing the –OCH₃ substituent is also extensively engaged in hydrophobic interactions with the side chains of residues Ile β 376, Leu β 253, and Ser β 239, thus satisfying the last (RA) pharmacophore feature. Finally, along the 20 ns MD trajectory another albeit intermittent hydrogen bond interaction is also detected between the oxygen atom of the –OCH₃ group and the –OH of Ser β 239 (ADL = 3.6 Å), which contributes to anchor the molecule in the proper, productive orientation within the binding site, thus contributing further to the high activity of this compound.

By resorting to the MM/PBSA approach we subsequently estimated the free energy of binding, ΔG_{bind} , for podophyllotoxin, colchicine, MDL 27048 and CHALC101 to human tubulin as a benchmark for our

computational procedure. Table 8 shows the binding free energy components averaged over the MD trajectory for each of these complexes: all ligands are correctly ranked for affinity, and the magnitudes of the calculated ΔG_{bind} values are in good agreement with the corresponding experimental evidences [43,44,48].

Furthermore, Table 8 shows the corresponding affinities of compounds (1–4 and 1a–3a) to the protein. If we examine the contributions to binding across our compounds we can see that, although both the electrostatic and the van der Waals interaction energy contributions are important for binding, the overall non-polar interactions ($\Delta E_{\text{MM}}^{\text{dW}} + \Delta G_{\text{sol}}^{\text{np}}$) constitute the driving force to tubulin binding for these molecules. Interestingly, and somewhat contrarily to what could be expected, the presence of the [1,3] dioxolo moiety in compound 4 does not afford a substantial favorable contribution to the dispersion energies compared to that of the other molecules (see Table 8), but mainly contributes to a molecular conformation amenable for fitting into the protein binding site. Further analysis of the ΔG_{bind} components reveals that while the van der Waals and non-polar solvation energies drive binding for all ligands, sterics alone do not completely explain the affinity differential. We also find that the overall electrostatic component to binding either provides no thermodynamic benefit or even opposes association despite the presence of some polar groups in the active site. Among the five modeled compounds, the two most effective ligands 1 and 4 have overall unfavorable electrostatic component to binding ($\Delta E_{\text{MM}}^{\text{ele}} + \Delta G_{\text{sol}}^{\text{ele}}$) equal to +2.9 kcal/mol and +1.3 kcal/mol, respectively. As mentioned above, it appears that 1 gains some internal electrostatic energy ($\Delta E_{\text{MM}}^{\text{ele}}$) by having the –CN and –OCH₃ groups that interact favorably with the –OH group of Thr β 312 and Ser β 239, respectively, whilst 4 counteracts the unfavorable desolvation term ($\Delta G_{\text{sol}}^{\text{ele}}$) by interacting with water molecules in the binding site (data not shown).

6.3. Projection of the free energy to each residue of tubulin

In order to gain extra insight into the possible mechanism of tubulin-drug binding, the values of ΔG_{bind} calculated from the

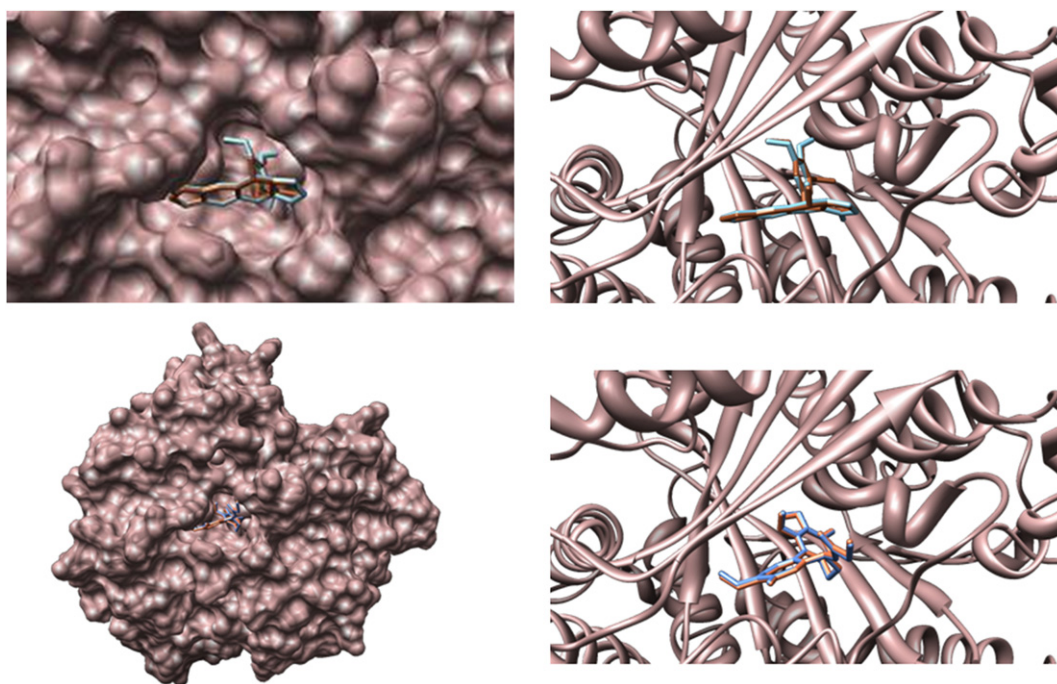


Fig. 6. Comparison between the co-crystallized (brown) and docked (light blue) structure of podophyllotoxin (top) and colchicine (bottom) into the allosteric binding site of human β -tubulin. Hydrogen atoms, water molecules, and counterions are omitted for clarity. Note that human β -tubulin and the crystallized *Bos Taurus* β -tubulin exhibit 98% sequential homology. (For interpretation of the references to colour in this figure legend, the reader is referred to the web version of this article.)

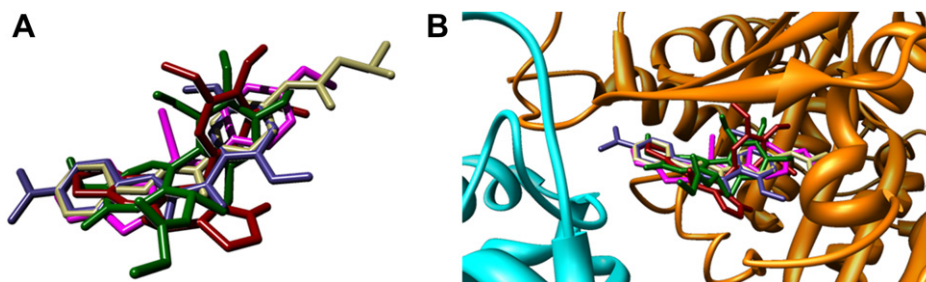


Fig. 7. (A) Superposition of the average structures of **1** (magenta), podophyllotoxin (dark red), colchicine (dark green), MDL 27048 (dark slate blue), and CHALC101 (dark kaki), and (B) detailed view of the superposed docked conformations of the same compounds in the allosteric binding site of tubulin. Hydrogen atoms, water molecules, and counterions are omitted for clarity. (For interpretation of the references to colour in this figure legend, the reader is referred to the web version of this article.)

MM/PBSA methodology were further decomposed into the nonbonded contribution afforded by individual tubulin binding site residues. As can be seen from Fig. 9, several residues belonging to the binding site responded differently to the different compounds. Further, the binding site residues not only impacted their own binding free energy interactions with the inhibitors but also influenced the interactions of other residues with the inhibitors by inducing slight alterations in the geometry of the binding site.

Favorable electrostatic interactions opposed by the polar solvation energy penalty also apply to individual residues. A change in electrostatic energy (ΔE_{MM}^{ele}) of any residue is always associated with an almost equal but opposite compensation in solvation energy (ΔG_{sol}), as illustrated in Fig. 10(A) for compounds **1–4** as an example. The correlation coefficients for all inhibitors range between 0.95 and 0.99. This high correlation between these two counteracting contributions to ΔG_{bind} made the change of the van der Waals nonbonded energy term ΔE_{MM}^{vdW} the largest factor in the loss of binding free energy between tubulin and all 3-Aryl-2-[1H-benzotriazol-1-yl]acrylonitrile derivatives. To highlight those residues with a significant difference between the lead compound **1** and all remaining inhibitors **2–4** and **1a–3a**, a cut-off of 1 kcal/mol of ΔE_{MM}^{vdW} was considered [49]. Thus, only those residues with a loss of van der Waals energy greater than the cut-off are plotted in Fig. 10 (B) and (C).

As can be seen by comparing Fig. 10 (B) and (C), some residues which are critical for the favorable binding in the case of the lead compound **1** (as well as for the other member of the series **2–4**), become unfavorable in the analogs bearing two chlorine atoms as substituents on the benzotriazole group (**1a–3a**). This information, coupled with the corresponding quantification of the van der Waals energy loss, as discussed below, can yield important information both for rationalizing the activity of the present molecules and the design of new microtubule destabilizing agents.

6.4. Van der Waals energy contribution from inhibitors

To further explore the mechanism of loss in free energy of binding between the different inhibitors and tubulin, the van der Waals contributions were calculated for each atom of each compound **2–4** and **1a–3a**, and compared to those relative to the lead molecule **1**. On average, each inhibitor has 35 atoms, 12 of which are hydrogens which afford a limited contribution to the dispersion energy term. Thus, we present and discuss data for the heavy atoms of each inhibitor only.

From the structural standpoint, both molecular series (**1–4** and **1a–3a**) can be considered formed by three major moieties: A) the benzotriazole group, B) the nitrile-substituted double bond, and C) the substituted phenyl ring (Fig. 11). To compare the energy variation between these three moieties for the different inhibitors, we defined a van der Waals energy variation index, VVI, as:

$$VVI = \frac{\sum_i (E_{vdW,i}^n - E_{vdW,i}^1)}{\sum_i E_{vdW,i}^1} \times 100 \quad (1)$$

in which i is the i -th atom within a specific moiety. Interestingly, the benzotriazole heterocycle has a relatively low and constant value of VVI in the series **2–4**, the same moiety being characterized by somewhat higher VVI values in compounds **1a–3a** (Table 9). On the other hand, both the phenyl ring and the double bond have significantly higher and more variable VVI values in compounds **1a–3a** with respect to the corresponding counterparts in compounds **2–4** (Table 9).

A deeper examination of the MD trajectories of each inhibitor in complex with tubulin reveals that, particularly when unsubstituted, the benzotriazole group maintains a relatively stable

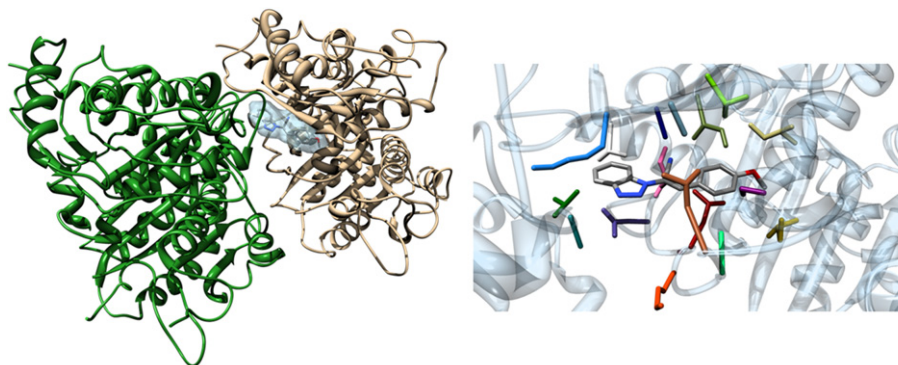


Fig. 8. Overall view of compound **1** in complex with tubulin (left) and detailed view of tubulin residues interacting with **1** (right). Tubulin residue color code: A α 180, dark cyan; V α 181, dark green; I β 236, dark kaki; S β 239, dark magenta; L β 240, gold; L β 246, sienna; A β 248, spring green; K β 252, orange red; L β 253, dark red; N β 256, dark slate blue; M β 257, hot pink; T β 312, white; A β 314, navy blue; V β 316, chartreuse; K β 350, dodger blue; A β 352, sky blue; I β 376, dark olive green. (For interpretation of the references to colour in this figure legend, the reader is referred to the web version of this article.)

Table 8
Free energy components, total binding energy ΔG_{bind} from molecular dynamics simulations on human tubulin in complex with compounds **1–4**, and **1a–3a**. The calculated values for the test compounds podophyllotoxin, colchicine, MDL 27048 and CHALC101 are also reported for comparison and validation.

Compd	$\Delta E_{MM}^{\text{ele}}$	$\Delta E_{MM}^{\text{vdW}}$	ΔE_{MM}	$\Delta C_{\text{sol}}^{\text{ele}}$	$\Delta C_{\text{sol}}^{\text{np}}$	ΔG_{sol}	$-T\Delta S$	ΔG_{bind}
1	-22.8 ± 0.3	-25.6 ± 0.2	-48.4 ± 0.2	25.7 ± 0.3	-2.5 ± 0.0	23.2 ± 0.3	16.9 ± 0.5	-8.3
2	-21.0 ± 0.2	-23.5 ± 0.1	-44.5 ± 0.1	23.3 ± 0.3	-2.8 ± 0.0	20.5 ± 0.3	16.2 ± 0.4	-7.8
3	-20.9 ± 0.2	-23.2 ± 0.2	-44.1 ± 0.2	23.7 ± 0.3	-2.9 ± 0.0	20.8 ± 0.3	16.3 ± 0.5	-7.0
4	-23.9 ± 0.3	-21.9 ± 0.2	-45.8 ± 0.2	25.2 ± 0.3	-2.9 ± 0.0	22.3 ± 0.3	15.8 ± 0.4	-7.7
1a	-21.1 ± 0.1	-20.8 ± 0.2	-41.9 ± 0.2	24.5 ± 0.3	-3.1 ± 0.0	20.5 ± 0.2	16.0 ± 0.4	-4.5
2a	-21.8 ± 0.2	-22.0 ± 0.1	-43.8 ± 0.1	23.8 ± 0.1	-2.9 ± 0.0	20.9 ± 0.1	16.6 ± 0.5	-6.3
3a	-21.9 ± 0.3	-21.6 ± 0.2	-43.5 ± 0.2	23.5 ± 0.4	-2.8 ± 0.0	-22.8 ± 0.3	16.7 ± 0.4	-6.1
Podophyllotoxin	-26.4 ± 0.3	-15.8 ± 0.2	-42.3 ± 0.2	27.2 ± 0.4	-4.1 ± 0.0	23.1 ± 0.4	$10.2 \pm$	-9.0
Colchicine	-27.4 ± 0.4	-20.4 ± 0.3	-47.8 ± 0.2	32.8 ± 0.6	-4.3 ± 0.0	28.5 ± 0.6	$9.1 \pm$	-10.2
MDL 27048	-29.5 ± 0.3	-23.8 ± 0.3	-53.4 ± 0.2	30.5 ± 0.3	-3.0 ± 0.0	27.5 ± 0.3	$17.4 \pm$	-8.5
CHALC101	-26.2 ± 0.2	-21.2 ± 0.2	-47.4 ± 0.1	26.6 ± 0.4	-2.8 ± 0.0	23.8 ± 0.4	$17.4 \pm$	-6.2

structure compared to the other two inhibitor main structural parts. This relative stability for inhibitors **1–4** with respect to **1a–3a** confirms that an unsubstituted benzotriazole group is essential to maintain important van der Waals interactions with the tubulin residues in most of the conformations that the molecules sample in their motions within the binding site. When two chlorine atoms replace two hydrogens on this heterocyclic scaffold, the free-energy decomposition coupled with VVI values clearly shows that more tubulin residues present considerable loss of van der Waals interactions with the inhibitors. This is particularly true when the $-\text{OCH}_3$ substituent on moiety C is no longer present to anchor the molecules via the important hydrogen bond with Ser β 239. A comparison of the relevant MD structure snapshots of **1**, **1a**, **2** and **2a** in complex with tubulin, taken as proof-of-concepts and illustrated in Fig. 12, shown that both moieties B and C in the **a** series of compounds undergo significant geometry changes within the binding site, that ultimately lead these groups to lose some of their van der Waals contacts with the protein binding pocket residues.

7. Conclusions

The results from antiproliferative screenings, reported in Table 2, show that no (*E*)-2-(5,6-dichloro-1*H*-benzo[d][1,2,3]triazol-1-yl)-3-(4-*R*-phenyl)acrylonitrile derivative **1a–3a** resulted more potent than its counterpart **1–3** as so as of **4**, thus proving that the introduction of chlorine atoms on the benzo-moiety decreases the antiproliferative activity of this class of benzotriazole derivatives.

Cell cycle analysis revealed that these series of compounds act on the G2/M phase of the cell cycle, an evidence consistent with a possible tubulin binding activity. This evidence was further

confirmed by competition experiments, in which compound **4** strongly displaced radio labeled colchicine from its binding site on the tubulin, showing an IC_{50} value lower than that of colchicine. Accordingly, the putative binding modes of these compounds on human β -tubulin were predicted using a combined 3D pharmacophore development/docking procedure, which was tested against the available crystal structures of tubulin in complex with known inhibitors. Further, the binding affinities of the lead compounds **1–4** and new molecules **1a–3a** were estimated using a computational ansatz that combines MM/PBSA and normal mode calculations. Importantly, the results stemming from the free energy calculations highlighted the dominant role of the van der Waals energy component ($\Delta E_{MM}^{\text{vdW}}$) to the overall ΔG_{bind} values, as the favorable electrostatic contribution to binding was almost counterbalanced by an almost equal but opposite desolvation term. Further, the decomposition of the free energy analysis on tubulin binding site residues indicated that, while the benzotriazole group in all compounds sustained their van der Waals interactions with most of the protein binding pocket, the other two moieties (i.e., the cyano-substituted double bond and the substituted phenyl ring) were able to sample a larger conformational space within the tubulin binding site, adopting several conformations that lose favorable dispersive interactions with important, anchor residues.

The combination of experimental and computational results presented in this paper support the hypothesis that this class of compounds can act as antiproliferative agents by interacting with tubulin in the colchicine binding sites. Consequently, they could inhibit tubulin assembly and might accordingly be classified as microtubule destabilizing agents. More, the modeling study proposes a rationale for the lower antiproliferative activity of the compound series **1a–3a** with respect to the leading series **1–4**, and

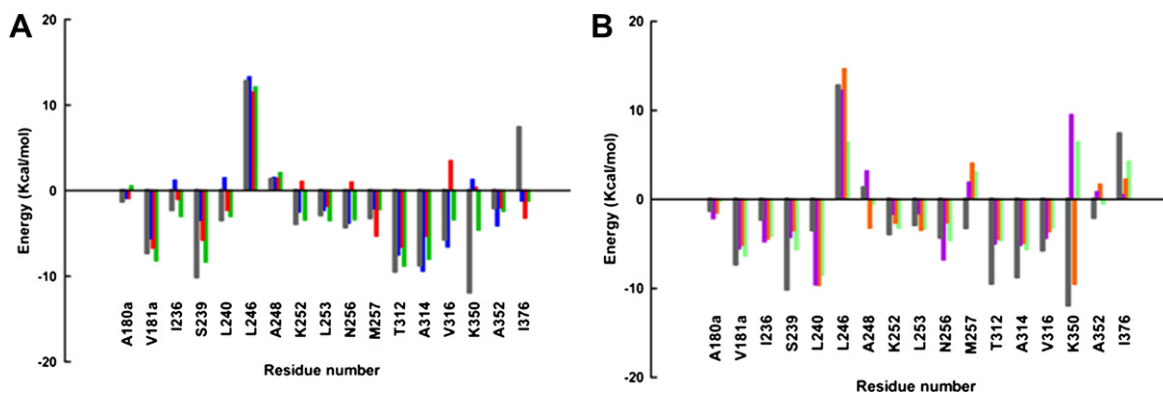


Fig. 9. Decomposition of energy from MM/PBSA per tubulin binding site residue. Total molecular mechanics ($\Delta E_{MM}^{\text{vdW}} + \Delta E_{MM}^{\text{ele}}$) energy component of each residue with (A) compounds **1** (gray), **2** (blue), **3** (red), and **4** (green), and (B) compounds **1** (gray), **1a** (violet), **2a** (orange), and **3a** (light green). (For interpretation of the references to colour in this figure legend, the reader is referred to the web version of this article.)

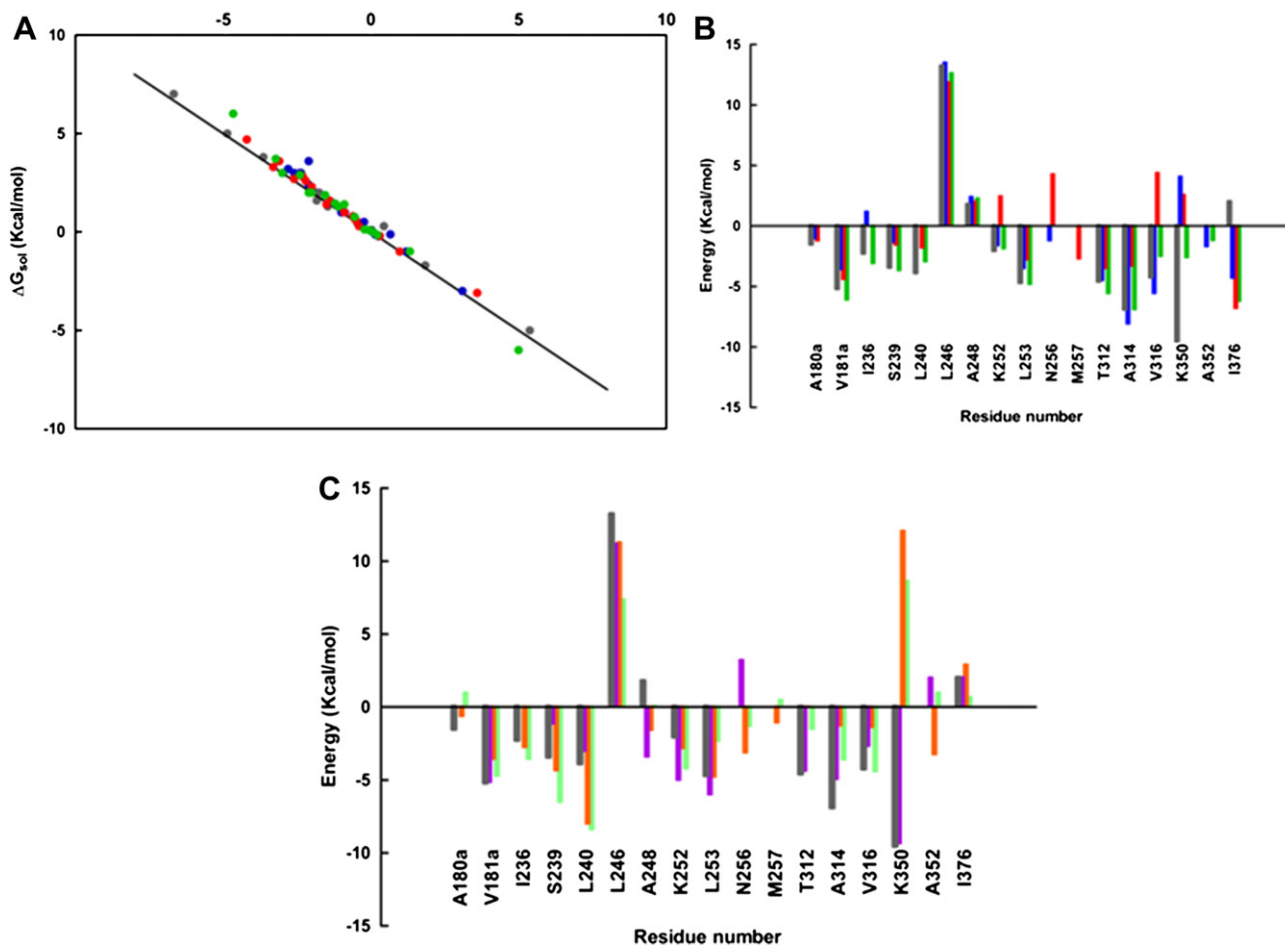


Fig. 10. (A) Correlation between the solvation (ΔG_{sol}) and electrostatic contribution (ΔE_{MM}^{elec}) of each tubulin binding site residue to the binding of compounds 1–4. Tubulin residues with van der Waals energy component larger than 1.0 kcal/mol interacting with (B) compounds 1 (gray), 2 (blue), 3 (red), and 4 (green), and (C) compounds 1 (gray), 1a (violet), 2a (orange), and 3a (light green). (For interpretation of the references to colour in this figure legend, the reader is referred to the web version of this article.)

suggests that the design of new tubulin-binding agents based on similar scaffolds should consider a careful balance between the choice of substituents on the benzotriazole moiety A and the re-optimization of the remaining molecular moieties B and C, as these two may not be longer able to maintain some critical interactions with tubulin by virtue of small albeit important conformational changes. Further biological and computational studies on other compounds will be reported in due course.

8. Materials and methods

8.1. Melting points, analytical and spectroscopical data

Melting points were determined by a Kofler hot stage or Digital Electrothermal apparatus, and are uncorrected. Infrared spectra are for Nujol mulls and were recorded using a Perkin–Elmer 781 spectrophotometer. UV spectra are qualitative and were recorded in nm for solutions in EtOH with a Perkin–Elmer Lambda 5 spectrophotometer. ^1H NMR spectra were recorded on a Varian XL-200 instrument, using TMS as internal standard. The chemical shift values are reported in ppm (δ) and coupling constants (J) in Hertz (Hz). Signal multiplicities are represented by: s (singlet) and d (doublet). MS spectra were performed on combined HP 5790–HP 5970 GC/MS apparatus. Column chromatography was performed using 230–400 mesh silica gel (Merck silica gel 60). Light

petroleum refers to the fraction with bp 40–60 °C. The analytical results for C, H, N and chlorine were within 0.4% of the theoretical values.

8.2. Preparation of 5,6-dichloro-1H-benzo[d][1,2,3]triazole (5)

Compound 5 was prepared following the procedure previously described [32].

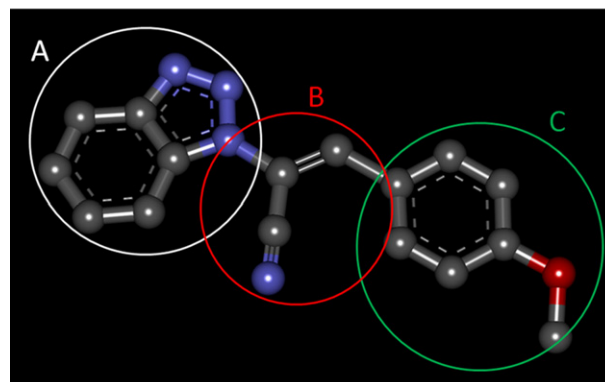


Fig. 11. Definition of the three main chemical moieties of compounds 1–4 and 1a–3a illustrated for compound 1 as an example.

Table 9
van der Waals energy variation index (VVI, %) for the three main moieties A, B, and C of compounds **2–4** and **1a–3a**.

Compd	A	B	C
2	3	7	4
3	3	8	7
4	5	8	5
1a	13	29	22
2a	9	21	18
3a	10	23	15

8.3. Preparation of 2-(5,6-dichloro-1H-benzo[d][1,2,3]triazol-1-yl)acetonitrile (**6a**) and 2-(5,6-dichloro-2H-benzo[d][1,2,3]triazol-2-yl)acetonitrile (**6b**)

2 g (10 mmol) of 5,6-dichloro-1H-benzo[d][1,2,3]triazole were dissolved in 20 ml of DMF. To this solution are added 1.18 g (11.7 mmol) 1.62 ml of triethylamine and 1.2 g (16 mmol) 1.02 ml of chloroacetonitrile. The whole mixture was heated under reflux for 12 h. After cooling, the triethylamine hydrochloride formed is filtered, and the solution is evaporated to dryness. Residue, dissolved in ether, is subjected to a series of washes with water. Evaporation of the extract is obtained a residue containing the two isomers **6a** and **6b**, that are separated by flash chromatography. Elution with light petroleum-ethyl acetate 80:20 afforded desired compounds: 2-(5,6-dichloro-1H-benzo[d][1,2,3]triazol-1-yl)acetonitrile (**6a**): yield: 23%; mp: 149–150 °C; IR (Nujol): ν_{\max} 2240 cm^{-1} ; UV(EtOH): λ_{\max} 217, 271, 292 nm; $^1\text{H NMR}$ (CDCl_3): δ 8.27 (s, 1H, H-4), 7.85 (s, 1H, H-7), 5.58 (s, 2H, CH_2); MS: m/z 226, 228, 230 (M^+). Anal. $\text{C}_8\text{H}_4\text{Cl}_2\text{N}_4$ (C, H, N). 2-(5,6-dichloro-2H-benzo[d][1,2,3]triazol-2-yl)acetonitrile (**6b**): yield: 15%; mp: 122–123 °C; IR (Nujol): ν_{\max} 2240 cm^{-1} , UV(EtOH) 219, 290, 302 nm; $^1\text{H NMR}$ (CDCl_3): δ 8.06 (s, 2H, H-4 e H-7), 5.64 (s, 2H, CH_2); MS: m/z 226, 228, 230 (M^+). Anal. $\text{C}_8\text{H}_4\text{Cl}_2\text{N}_4$ (C, H, N).

8.4. Preparation of (E)-2-(5,6-dichloro-1H-benzo[d][1,2,3]triazol-1-yl)-3-(4-R-phenyl)acrylonitriles (**1a**, **2a**, **3a**)

8.4.1. (E)-2-(5,6-dichloro-1H-benzo[d][1,2,3]triazol-1-yl)-3-(4-methoxyphenyl)acrylonitrile (**1a**)

To a solution of 2-(5,6-dichloro-1H-benzo[d][1,2,3]triazol-1-yl)acetonitrile (**6a**) (1.32 mmol) and Et_3N (4.0 mmol) in toluene (5 mL)

stirred at room temperature, a solution of 4-methoxybenzaldehyde (2.31 g, 17 mmol) in the same solvent (3 mL) was added dropwise. After addition was complete, the whole mixture was heated under reflux for 24 h. The desired compound (only *E* isomer), was obtained by chromatography on silica gel column, eluting by light petroleum-ethyl acetate 70:30 of the crude residue obtained after evaporation of the toluene solution. Yield 40%; M.p. 193–194 °C (acetone); IR (Nujol): ν 2219 (CN) cm^{-1} ; UV (EtOH): λ_{\max} 318, 353 nm; $^1\text{H NMR}$ (CDCl_3): δ 8.26 (s, 1H, H-4), 8.04 (s, 1H, H-7), 7.93 (d, $J = 8.4$, 2H, H-2' + H-6'), 7.81 (s, 1H, vinyl-H), 7.04 (d, $J = 8.4$, 2H, H-3' + H-5'), 3.92 (s, 3H, OCH_3); MS: m/z 344, 346, 348 (M^+); Anal. $\text{C}_{16}\text{H}_{10}\text{Cl}_2\text{N}_4\text{O}$ (C, H, N).

8.4.2. (E)-2-(5,6-dichloro-1H-benzo[d][1,2,3]triazol-1-yl)-3-*p*-tolylacrylonitrile (**2a**)

To a solution of 2-(5,6-dichloro-1H-benzo[d][1,2,3]triazol-1-yl)acetonitrile (**6a**) (1.32 mmol) and Et_3N (4.0 mmol) in toluene (5 mL) stirred at room temperature, a solution of 4-methylbenzaldehyde (2.04 g, 17 mmol) in the same solvent (3 mL) was added dropwise. After addition was complete, the whole mixture was heated under reflux for 24 h. The desired compound (only *E* isomer), was obtained by chromatography on silica gel column, eluting by light petroleum-ethyl acetate 80:20 of the crude residue obtained after evaporation of the toluene solution. Yield: 20%; mp: 105–107 °C (acetone); IR (Nujol): ν 2214 (CN) cm^{-1} ; UV (EtOH): λ_{\max} 221, 297, 330 nm; $^1\text{H NMR}$ (CDCl_3): δ 8.27 (s, 1H, H-4), 8.06 (s, 1H, H-7), 7.88 (s, 1H, vinyl-H), 7.84 (d, $J = 8.4$, 2H, H-2' + H-6') 7.36 (d, $J = 8.4$, 2H, H-3' + H-5'), 2.47 (s, 3H, CH_3); MS: m/z 328, 330, 332 (M^+); Anal. $\text{C}_{16}\text{H}_{10}\text{Cl}_2\text{N}_4$ (C, H, N).

8.4.3. (E)-3-(4-bromophenyl)-2-(5,6-dichloro-1H-benzo[d][1,2,3]triazol-1-yl)acrylonitrile (**3a**)

To a solution of 2-(5,6-dichloro-1H-benzo[d][1,2,3]triazol-1-yl)acetonitrile (**6a**) (0.3g, 1.32 mmol) and Et_3N (4.0 mmol) in toluene (5 mL) stirred at room temperature, a solution of 4-bromobenzaldehyde (3.14 g, 17 mmol) in the same solvent (3 mL) was added dropwise. After addition was complete, the whole mixture was heated under reflux for 24 h. The desired compound was obtained by filtration of the resulting precipitates as soon as the reaction mixture reaches r.t. Yield 33%; m.p. 150–152 °C (acetone); IR (Nujol): ν 2225 (CN) cm^{-1} ; UV (EtOH): λ_{\max} 216, 297 nm; $^1\text{H NMR}$ (CDCl_3): δ 8.36 (s, 1H, H-4), 8.27 (s, 1H, H-7), 8.14 (s,

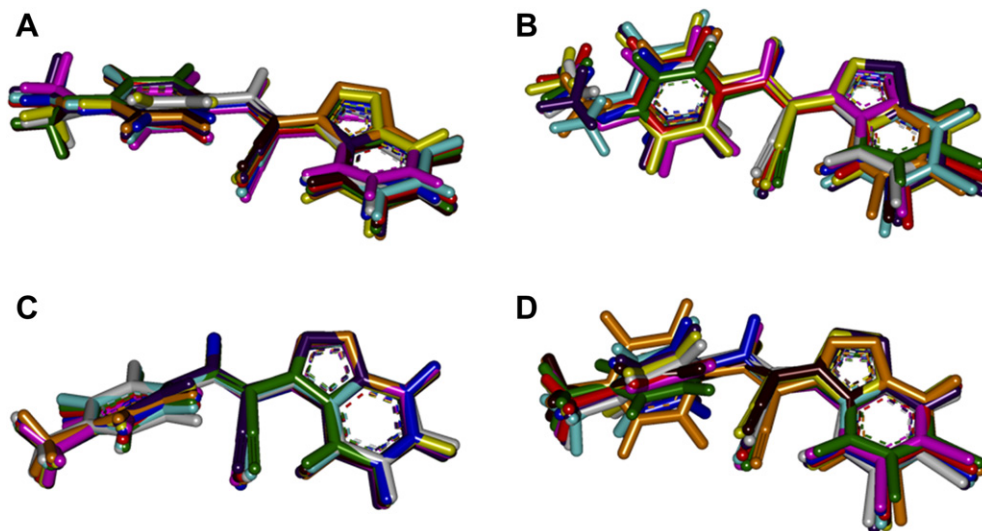


Fig. 12. Conformational space of (A) compound **1**, (B) **1a**, (C) **2**, and (D) **2a** sampled in their complex with tubulin by MD simulations. For each compound, only 10 representative snapshots taken along the corresponding MD trajectories are shown in different colors for clarity.

1H, vinyl-H), 7.92 (d, $J = 8.2$, 2H, H-2' + H-6') 7.72 (d, $J = 8.6$, 2H, H-3' + H-5'), 3.27 (s, 3H, CH₃); MS: m/z 392, 394, 396, 397, 399 (M⁺); Anal. C₁₅H₇BrCl₂N₄(C, H, N).

8.5. Cell-based assay

Test compounds were dissolved in DMSO at 100 mM and then diluted into culture medium.

8.5.1. Cells

Cell lines were purchased from American Type Culture Collection (ATCC). Hematological tumor-derived cell lines were grown in RPMI-1640 medium supplemented with 10% FCS, 100 units/mL penicillin G and 100 μg/mL streptomycin. Solid tumor-derived cell lines were grown in their specific media supplemented with 10% FCS and antibiotics. Cell cultures were incubated at 37 °C in a humidified, 5% CO₂ atmosphere. The absence of mycoplasma contamination was checked periodically by the Hoechst staining method.

8.5.2. Antiproliferative assays

Exponentially growing cells derived from human hematological tumors [CD4⁺ human T-cells containing an integrated HTLV-1 genome (MT-4); CD4⁺ human acute T-lymphoblastic leukemia (CCRF-CEM); Human splenic B-lymphoblastoid cells (WIL-2NS); Human acute B-lymphoblastic leukemia (CCRF-SB)] were seeded at an initial density of 1×10^5 cells/mL in 96 well plates in RPMI-1640 medium supplemented with 10% fetal calf serum (FCS), 100 units/mL penicillin G and 100 μg/mL streptomycin. Human cell lines derived from solid tumors [skin melanoma (SK-MEL-28); breast adenocarcinoma (MCF-7); lung squamous carcinoma (SK-MES-1); hepatocellular carcinoma (HepG-2) and prostate carcinoma (DU-145)] were also seeded at 1×10^5 cells/mL in 96 well plates in specific media supplemented with 10% FCS and antibiotics as above. Cell cultures were then incubated at 37 °C in a humidified, 5% CO₂ atmosphere in the absence or presence of serial dilutions of test compounds. Cell viability was determined after 96 h at 37 °C by the 3-(4,5-dimethylthiazol-2-yl)-2,5-diphenyl-tetrazolium bromide (MTT) method [50].

8.5.3. Analysis of cell cycle

Cells were washed once in ice-cold PBS and resuspended at 1×10^6 ml in a hypotonic fluorochrome solution containing propidium iodide (Sigma) 50 μg/ml in 0.1% sodium citrate plus 0.03% (v/v) nonidet P-40 (Sigma). After 30 min of incubation the fluorescence of each sample was analyzed as single-parameter frequency histograms using a FACS can flow cytometer (Becton–Dickinson, San Jose, CA). Distribution of cells in cell cycle was determined using the ModFit LT program (Verity Software House, Inc.). Apoptosis was determined by evaluating the percentage of hypoploid nuclei accumulated in the sub-G₀–G₁ peak after labeling with propidium iodide.

8.6. [³H]Colchicine competition-binding scintillation proximity assay (SPA) [34]

[³H]Colchicine was diluted, and biotin-labeled tubulin (T333, Cytoskeleton, Denver, CO) was reconstituted following the manufacturer protocol. The diluted compound **4** and [³H]colchicine were transferred to a 96-well isoplate (PE-Wallac, Boston, MA), to which the binding buffer and the reconstituted biotinylated tubulin were added. The plates were incubated at 37 °C for 2 h; then, streptavidin-coated yttrium SPA beads (Amersham Pharmacia Biotech, Piscataway, NJ) were added, and the bound radioactivity was determined using a MicroBetaTriluxMicroplate Scintillation

Counter (PE-Wallac Boston, MA). IC₅₀ values were calculated via data non-linear regression using GraphPad Prism 5.

8.7. Molecular modeling

The extensive, parallel molecular dynamics analyses were performed using 64 processors of the Tartaglia cluster at the University of Trieste (Trieste, Italy), as well as the same number of processors on the IBM/BX cluster at the CINECA supercomputer center (Bologna, Italy). The *Catalyst* module of the *Discovery Studio* platform [37] was employed for 3D pharmacophore model development. The software *AutoDock* [51] was used for ligand docking. The parallel version of the *Amber 9* suite of programs [52] was employed in all molecular dynamics simulations. Molecular graphics images were produced using the UCSF *Chimera* package from the Resource for Biocomputing, Visualization, and Informatics at the University of California, San Francisco (supported by NIH P41 RR-01081) [53].

8.7.1. 3D pharmacophore model generation

For the automated pharmacophore generation with *DS Catalyst*, a training set of 25 inhibitors of tubulin, with CC₅₀ values between 0.05 and 20,000 μM, was defined (Table 5). The test set used for the validation of the pharmacophore model consisted of further 11 derivatives, as reported in Table 6. The details of the pharmacophore development procedure with *Catalyst* have been extensively described in previous work [49,54–57]. Briefly, the model structures of all compounds were sketched and each molecular structure was subjected to energy minimization using the generalized CHARMM force field [58] until the gradient dropped below 0.05. A conformational search was then carried out using the Poling algorithm [59–61] and the CHARMM force field as implemented in the *Catalyst* program. The “best quality” generation option was adopted to select representative conformers over a 0–20 kcal/mol interval above the computed global energy minimum in the conformational space, and the number of conformers generated for each compound was limited to a maximum of 250 as a good compromise between speed and maximum coverage in the conformational space.

Based on the conformations for each compound, the *HypoGen* module of *DS Catalyst* was used to generate three-dimensional pharmacophore models. During hypotheses generation, the software attempts to minimize a cost function of two main terms: the first penalizes the deviation between the estimated affinities of the training set molecules and their experimental values, whilst the second penalizes the complexity of the hypothesis. The uncertain factor for each compound represents the ratio range of uncertainty in the affinity value based on the expected statistical straggling of biological data collection. Uncertainty influences the first step – also called the constructive phase – of the hypothesis generating process. In this work, the default factor of 3.0 was selected, as the experimental affinities of our compounds span more than the required four orders of magnitude.

As the *DS Catalyst* software can generate pharmacophore hypotheses consisting of a maximum of five hypotheses, an initial analysis revealed that chemical feature types such as hydrogen bond acceptor (HBA), hydrogen bond donor (HBD), hydrophobic aromatic (HYAr), ring aromatic (RA), and general hydrophobic (HY) sites could effectively map all critical chemical features of all molecules in the training and test sets. Accordingly, these five feature types were used to generate 10 pharmacophores from the training set.

The *HypoGen* module in *DS Catalyst* performs two important cost calculations (represented in bit units) that determine the success of any pharmacophore hypothesis. One is called the *fixed cost*, which represents the simplest model that fits all data perfectly, while the

second is known as the null cost, and represents the highest cost of a pharmacophore with no features and which estimates activity to be the average of the activity data of the training set molecules. A meaningful pharmacophore hypothesis may result when the difference between these two values is large; for instance, a value of 40–60 bits for a 3D pharmacophore hypothesis may indicate that it has 75–90% probability of correlating the data. Also, the total cost of any pharmacophore hypothesis should be close to the fixed cost to provide any useful model. A further parameter that also determines the quality of a given 3D pharmacophore model with possible predicting value is the configurational cost, also known as the entropy cost and depends on the complexity of the pharmacophore hypothesis space. For a good hypothesis, this cost, that is the magnitude of the hypothesis space for a given training set of compounds, should be less than 17. If this last cost exceeds 17, there are more degrees of freedom in the training set that the *DS Catalyst* algorithm can properly handle and, consequently, the corresponding pharmacophore is likely to be poorly meaningful. Finally, the root-mean-square deviations (RMSDs) and the correlation coefficients ρ represent *de facto* the quality of the correlation between the estimated and the actual activity data.

Three validation procedures were followed to determine the statistical relevance and the validity of the proposed 3D pharmacophore models: the *test set* prediction model, the *randomization* method, and the *leave-one-out* procedure. In this work, the former procedure consisted in the collection of further, different compounds into a test set, and in performing a regression analysis by mapping the test set molecules onto the best pharmacophore hypothesis. The high correlation coefficients obtained using the test set compounds revealed the good correlation between the actual and estimated affinities and, hence, the predictive validity of the corresponding 3D hypothesis. The *randomization* validation procedure is based on Fisher's randomization test [39]. The goal of this type of validation is to check whether there is a strong correlation between the chemical structures and the biological activity. This is done by randomizing the affinity data associated with the training set compounds, generating pharmacophore hypothesis using the same features and parameters employed to develop the original pharmacophore model. The statistical significance is calculated according to the following formula:

$$\text{Significance} = 100 \times \left[\hat{I}(1 + x/y) \right]$$

where x is the total number of hypotheses having a total cost lower than the original (best) hypothesis, and y is the total number of HypoGen runs (initial + random runs). Thus, for instance, 99 random spreadsheets (i.e., 99 HypoGen runs) have to be generated to obtain a 99% confidence level. Should any randomized data set result in the generation of a 3D pharmacophore with similar or even better cost values, root-mean-square deviations, and correlation coefficients, then it is likely that the original hypothesis does reflect a chance correlation.

Finally, the *leave-one-out* test checks if the correlation between experimental and computed affinities is heavily dependent on one particular molecule of the training set by re-computing the pharmacophore model with the exclusion of one molecule at a time. Accordingly, 24 new training sets were built, each composed by 23 molecules, and 24 HypoGen calculations were launched under the same conditions. For each run, the hypothesis characterized by the lowest total cost was employed to predict the affinity of the excluded compound and to estimate the new correlation coefficient.

8.7.2. Molecular docking studies

The 3D model structure of human β -tubulin, presently not available in the Protein Data Bank (PDB), was built by a combination

of homology-based techniques [62]. Briefly, we used the *Discovery Studio* software (v.2.1, Accelrys Inc., San Diego, CA, USA) to generate a sequence alignment among model protein (human β -tubulin, SwissProt accession code Q9H4B7) and three reference proteins (i.e., Bos Taurus, Sus Scrofa, and Ovis Aries tubulin β -chains, PDB entry codes 1SA1, 1IAO, and 3HKC, respectively). Subsequently, the Modeler program [63,64] was employed to build a preliminary 3D model of human tubulin β -chain based on the alignment obtained in the previous step. The model generated was further refined using statistical pair potentials for the loops. The geometry of protein was refined for 200 steps (steepest descent) in vacuum, using the all-atom the *ff03* force field of Duan et al. [65,66] as defined in *parm99.dat* and *frmod.ff03* parameter files [67]. Further protein geometry refinement was carried out using the *PMEMD* module of *Amber 9* via a combined steepest descent – conjugate gradient algorithm, using as a convergence criterion for the energy gradient the root-mean-square of the Cartesian elements of the gradient equal to 10^{-2} kcal/(mol Å). The quality of the model was assessed by using different validation tools such as *Procheck* [68] and *Whatif* [69]. Ramachandran plot statistics indicated that 98% of the main-chain dihedral angles were found in the most favorable region, thus confirming the exceptional quality of the 3D model of human β -tubulin obtained. This optimized 3D model was then used as the entry point for molecular dynamics (MD) simulations.

The model structures of the selected ligands were generated with *Discovery Studio*. All molecules were subjected to an initial energy minimization, with the convergence criterion set to 10^{-4} kcal/(mol Å). A conformational search was carried out using a well-validated, ad-hoc developed combined molecular mechanics/molecular dynamics simulated annealing (MDSA) protocol [45,46,62,70]. Accordingly, the relaxed structures were subjected to 5 repeated temperature cycles (from 310 K to 1000 K and back) using constant volume/constant temperature (NVT) MD conditions. At the end of each annealing cycle, the structures were again energy minimized to converge below 10^{-4} kcal/(mol Å), and only the structures corresponding to the minimum energy were used for further modeling. The atomic partial charges for the geometrically optimized compounds were obtained using the RESP procedure [71], and the electrostatic potentials were produced by single-point quantum mechanical calculations at the Hartree-Fock level with a 6-31G* basis set, using the Merz-Singh-Kollman van der Waals parameters [72,73]. Eventual missing force field parameters for the inhibitor molecules were generated using the *Antichamber* module of *Amber 9.0*.

The optimized structures of the test compounds were docked into the colchicin - podophyllotoxin binding site of tubulin by applying a consolidated procedure [74], accordingly, it will be described here only briefly. The software AutoDock4 [51] was employed to estimate the possible binding orientations of all compounds in the receptor. In order to encase a reasonable region of the protein surface and interior volume, centered on the crystallographic identified binding site (as determined by superposition with the highly homolog Bos Taurus β -tubulin in complex with colchicines, PDB entry 1SA0.pdb), the grids were 60 Å on each side. Grid spacing (0.375 Å), and 120 grid points were applied in each Cartesian direction so as to calculate mass-centered grid maps. Amber 12–6 and 12–10 Lennard–Jones parameters were used in modeling van der Waals interactions and hydrogen bonding (N–H, O–H and S–H), respectively. In the generation of the electrostatic grid maps, the distance-dependent relative permittivity of Mehler and Solmajer was applied [75].

For the docking of each compound to the protein, three hundred Monte Carlo/Simulated Annealing (MC/SA) runs were performed, with 100 constant temperature cycles for simulated annealing. For these calculations, the GB/SA implicit water model [76,77] was used to mimic the solvated environment. The rotation of the angles ϕ

and ϕ , and the angles of side chains were set free during the calculations. All other parameters of the MC/SA algorithm were kept as default. Following the docking procedure, the structure of all compounds were subjected to cluster analysis with a tolerance of 1 Å for an all-atom root-mean-square (RMS) deviation from a lower-energy structure representing each cluster family. In the absence of any relevant crystallographic information, the structure of each resulting complex characterized by the lowest interaction energy in the prevailing cluster was selected for further evaluation.

Each best substrate/tubulin complex resulting from the automated docking procedure was further refined in *Amber 9* using the quenched molecular dynamics (QMD) method [70,78,79]. In this case, 1 ns molecular dynamics (MD) simulation at 310 K were employed to sample the conformational space of the substrate–tubulin complex in the GB/SA continuum solvation environment [76,77]. The integration step was equal to 1 fs. After each ps, the system was cooled to 0 K, the structure was extensively minimized, and stored. To prevent global conformational changes of the protein, the backbone of the protein binding site were constrained by a harmonic force constant of 100 kcal/Å, whereas the amino acid side chains and the ligands were allowed moving without any constraint.

The best energy configuration of each complex resulting from the previous step was allowed to relax in an 80 Å × 80 Å × 80 Å box of TIP3P water molecules [80]. The resulting system was minimized with a gradual decrease in the position restraints of the protein atoms. Finally, to achieve electroneutrality, a suitable number of counterions were added, in the positions of largest electrostatic potential, as determined by the module *LEaP* module within *Amber 9*. After energy minimization of the added ions for 1500 steps, keeping the protein, the ligand, and the pre-existing waters rigid, followed by an MD equilibration of the entire water/ion box with fixed solute for 2 ns, further unfavorable interactions within the structures were relieved by progressively smaller positional restraints on the solute (from 25 to 0 kcal/(mol Å²) for a total of 4 ns. Each hydrated complex system was gradually heated to 310 K in three intervals, allowing a 2 ns interval per each 100 K, and then equilibrated for 5 ns at 310 K, followed by 20 ns of data collection runs, necessary for the estimation of the free energy of binding (*vide infra*). The MD simulations were performed at constant $T = 310$ K using the Berendsen et al. coupling algorithm [81] with separate coupling of the solute and solvent to the heat, an integration time step of 2 fs, and the applications of the Shake algorithm [82] to constrain all bonds to their equilibrium values, thus removing high frequency vibrations. Long-range nonbonded van der Waals interactions were truncated by using a dual cut-off of 9 and 13 Å, respectively, where energies and forces due to interactions between 9 and 13 Å were updated every 20 time steps. The particle mesh Ewald method [83] was used to treat the long-range electrostatics. For the calculation of the binding free energy between tubulin and each inhibitor in water, a total of 20,000 snapshots were saved during the MD data collection period described above.

8.7.3. Free energy of binding

The binding free energy ΔG_{bind} of each tubulin/drug complex in water was calculated according to the procedure termed Molecular Mechanics/Poisson–Boltzmann Surface Area (MM/PBSA), and originally proposed by Srinivasan et al. [40]. Since the theoretical background of this methodology is described in details in the original papers by Peter Kollman and his group [84], it will be only briefly described below.

Basically, an MD simulation (typically in explicit solvent) is first carried out which yields a representative ensemble of structures. The average total free energy of binding between each drug and the protein receptor can then be calculated as:

$$\Delta G_{\text{bind}} = \Delta E_{MM} + \Delta G_{\text{solv}} - T\Delta S \quad (2)$$

where ΔG_{bind} is the binding free energy in water, ΔE_{MM} is the interaction energy between the ligand and the protein, ΔG_{solv} is the solvation free energy, and $-T\Delta S$ is the conformational entropy contribution to the binding. ΔE_{MM} is calculated from the molecular mechanics (MM) interaction energies, according to:

$$\Delta E_{MM} = \Delta E_{MM}^{\text{ele}} + \Delta E_{MM}^{\text{vdw}} \quad (3)$$

where $\Delta E_{MM}^{\text{ele}}$ and $\Delta E_{MM}^{\text{vdw}}$ are electrostatic and van der Waals interaction energies between the ligand and the receptor, which are calculated using the *MM/PBSA* module in the *Amber 9* software suite.

The solvation energy, ΔG_{solv} , is divided into two parts, the electrostatic contributions, $\Delta G_{\text{solv}}^{\text{ele}}$, and all other contributions, $\Delta G_{\text{solv}}^{\text{np}}$:

$$\Delta G_{\text{solv}} = \Delta G_{\text{solv}}^{\text{ele}} + \Delta G_{\text{solv}}^{\text{np}} \quad (4)$$

The electrostatic contribution to the solvation free energy, $\Delta G_{\text{solv}}^{\text{ele}}$, is calculated using the *DelPhi* software package [85], which solves the Poisson–Boltzmann equations numerically and calculates the electrostatic energy according to the electrostatic potential. Interior and exterior dielectric constant values ϵ were set equal to 1 and 80, respectively. A grid spacing of 2/Å, extending 20% beyond the dimensions of the solute, was employed. The non-polar component $\Delta G_{\text{solv}}^{\text{np}}$ was obtained using the following relationship [86]: $\Delta G_{\text{solv}}^{\text{np}} = \gamma \times SA + \beta$, in which $\gamma = 0.00542$ kcal/(mol Å²), $\beta = 0.92$ kcal/mol, and the surface area SA was estimated by means of the *MSM* software [87]. The last parameter in Equation (1), i.e. the change in solute entropy upon association $-T\Delta S$, was calculated through normal mode analysis [88], using the *N mode* module of *Amber 9*. In the first step of this calculation, an 8 Å sphere around the ligand was cut out from an MD snapshot for each ligand–protein complex. This value was shown to be large enough to yield converged mean changes in solute entropy. On the basis of the size-reduced snapshots of the complex, we generated structures of the uncomplexed reactants by removing the atoms of the protein and ligand, respectively. Each of those structures was minimized, using a distance-dependent dielectric constant $\epsilon = 4r$, to account for solvent screening, and its entropy was calculated using classical statistical formulas and normal mode-analysis. To minimize the effects due to different conformations adopted by individual snapshots we averaged the estimation of entropy over 40 snapshots.

Finally, the IC_{50} values were calculated from the corresponding binding free energies using the following relationship [41,42]:

$$\Delta G_{\text{bind}} = RT \ln K_{\text{diss}} = RT \ln (IC_{50} + 0.50C_{\text{enz}}) \cong RT \ln IC_{50} \quad (5)$$

The overall quality of the entire procedure described above – i.e., protein and inhibitors modeling, conformational analysis, docking and energetic calculations – was tested by carrying out the same calculations on podophyllotoxin, colchicines, MDL 27048, and CHALC101, for which the crystallographic structures of the relevant tubulin complexes and/or the corresponding IC_{50} values were available [40,41,45].

References

- [1] B.G. Szczepankiewicz, G. Liu, H.S. Jae, A.S. Tasker, I.W. Gunawardana, T.W. von Geldern, S.L. Gwaltney 2nd, J.R. Wu-Wong, L. Gehrke, W.J. Chiou, R.B. Credo, J.D. Alder, M.A. Nukkala, N.A. Zielinski, K. Jarvis, K.W. Mollison, D.J. Frost, J.L. Bauch, Y.H. Hui, A.K. Claiborne, Q. Li, S.H. Rosenberg, *J. Med. Chem.* 44 (2001) 4416–4430.
- [2] O. Valiron, N. Caudron, *D. Job, Cell. Mol. Life Sci.* 58 (2001) 2069–2084.
- [3] S. Sengupta, S.A. Thomas, *Expert Rev. Anticancer Ther.* 6 (2006) 1433–1447.
- [4] Y.K. Chiang, C.C. Kuo, Y.S. Wu, C.T. Chen, M.S. Coumar, J.S. Wu, H.P. Hsieh, C.Y. Chang, H.Y. Jseng, M.H. Wu, J.S. Leou, J.S. Song, J.Y. Chang, P.C. Lyu, Y.S. Chao, S.Y. Wu, *J. Med. Chem.* 52 (2009) 4221–4233.

- [5] A.R. Katritzky, *Farmaco* 43 (1988) 1175–1181.
- [6] A.R. Katritzky, S. Rachwal, G.J. Hitchings, *Tetrahedron* 47 (1991) 2683–2732.
- [7] A.R. Katritzky, J. Jiang, J.V. Greenhill, P.J. Steel, *J. Chem. Soc. Perkin Trans. 1* (1992) 3055–3060.
- [8] F. Sparatore, F. Pagani, *Farmaco Ed. Sci.* 17 (1962) 414–429.
- [9] F. Sparatore, F. Pagani, *Farmaco Ed. Sci.* 20 (1965) 248–258.
- [10] F. Sparatore, M.I. La Rotonda, G. Paglietti, E. Ramundo, C. Silipo, A. Vittoria, *Farmaco Ed. Sci.* 33 (1978) 901–922.
- [11] F. Sparatore, F. Pagani, G. Caliendo, E. Novellino, C. Silipo, A. Vittoria, *Farmaco Ed. Sci.* 43 (1988) 141–151.
- [12] A. Boido, I. Vazzana, F. Sparatore, B. Cappello, V. Diurno, C. Matera, R. Marrazzo, S. Russo, M.L. Cenicola, E. Marmo, *Farmaco* 44 (1989) 257–277.
- [13] M. Loriga, G. Paglietti, F. Sparatore, G. Pinna, A. Sisini, *Farmaco* 47 (1992) 439–448.
- [14] G. Paglietti, P. Sanna, A. Carta, F. Sparatore, I. Vazzana, A. Peana, M. Satta, *Farmaco* 49 (1994) 693–702.
- [15] I. Vazzana, A. Boido, F. Sparatore, R. Di Carlo, G. Mattace Raso, M. Pacilio, *Farmaco* 52 (1997) 131–139.
- [16] G. Paglietti, F. Sparatore, *Farmaco Ed. Sci.* 27 (1972) 380–396.
- [17] G. Paglietti, F. Sparatore, *Ann. Chim.* 62 (1972) 128–143.
- [18] A. Carta, P. Sanna, G. Paglietti, F. Sparatore, *Heterocycles* 55 (2001) 1133–1140.
- [19] P. Sanna, A. Carta, G. Paglietti, S. Zanetti, G. Fadda, *Farmaco* 47 (1992) 1001–1019.
- [20] P. Sanna, A. Carta, G. Paglietti, A. Bacchi, G. Pelizzi, *J. Heterocyclic Chem.* 34 (1997) 97–106.
- [21] A. Carta, P. Sanna, H. Molinari, *Heterocycles* 45 (1997) 1391–1395.
- [22] P. Sanna, A. Carta, G. Paglietti, *Heterocycles* 51 (1999) 2171–2181.
- [23] A. Carta, P. Sanna, A. Bacchi, *Heterocycles* 57 (2002) 1079–1090.
- [24] P. Sanna, A. Carta, M.E. Rahbar Nikookar, *Eur. J. Med. Chem.* 35 (2000) 535–543.
- [25] P. Sanna, A. Carta, L. Gherardini, M.E. Rahbar Nikookar, *Farmaco* 57 (2002) 79–87.
- [26] A. Carta, P. Sanna, M. Palomba, L. Vargiu, M. La Colla, R. Loddo, *Eur. J. Med. Chem.* 37 (2002) 891–900.
- [27] A. Carta, M. Palomba, G. Boatto, B. Busonera, M. Mureddu, R. Loddo, *Farmaco* 59 (2004) 637–644.
- [28] Y. Schneider, P. Chabert, J. Stutzmann, D. Coelho, A. Fougerousse, F. Gossé, J.F. Launay, R. Brouillard, F. Raul, *Int. J. Cancer* 107 (2003) 189–196.
- [29] R. Romagnoli, P.G. Baraldi, M.G. Pavani, M.A. Tabrizi, D. Preti, F. Fruttarolo, L. Piccagli, M.K. Jung, E. Hamel, M. Borgatti, R. Gambari, *J. Med. Chem.* 49 (2006) 3906–3915.
- [30] R. Romagnoli, P.G. Baraldi, M.G. Pavani, M.A. Tabrizi, D. Preti, F. Fruttarolo, L. Piccagli, M.K. Jung, E. Hamel, M. Borgatti, R. Gambari, *J. Med. Chem.* 49 (2006) 6425–6428.
- [31] M. Belleri, D. Ribatti, S. Vicoli, F. Cotelli, L. Forti, V. Tannini, L.A. Stivala, M. Presta, *Mol. Pharmacol.* 67 (2005) 1451–1459.
- [32] A. Carta, M. Loriga, S. Piras, G. Paglietti, M. Ferrone, M. Fermeglia, S. Prici, P. La Colla, G. Collu, T. Sanna, R. Loddo, *Med. Chem.* 3 (2007) 520–532.
- [33] Z. Xiao, K.F. Bastow, J.R. Vance, R.S. Sidwell, H.K. Wang, M.S. Chen, Q. Shi, K.H. Lee, *J. Med. Chem.* 47 (2004) 5140–5148.
- [34] S.K. Tahir, P. Kovar, S.H. Rosenberg, Ng Shi-Chung, *BioTechniques* 29 (2000) 156–160.
- [35] R. Bai, M.C. Roach, S.K. Jayaram, J. Barkoczy, G.R. Pettit, R.F. Luduena, E. Hamel, *Biochem. Pharmacol.* 45 (1993) 1503–1515.
- [36] R. Bai, G.R. Pettit, E.J. Hamel, *Biol. Chem.* 265 (1990) 17141–17149.
- [37] *Discovery Studio v. 3.0*, Accelrys, San Diego, CA, USA.
- [38] J. Sutter, O.F. Guner, R.D. Hoffman, H. Li, M. Wadman, in: O.F. Guner (Ed.), *Pharmacophore Perception, Development, and Use in Drug Design*, International University Line, La Jolla, CA, 1999, pp. 501–511.
- [39] R. Fisher, *The Design of Experiments*. Hafner Publishing, New York, NY, USA, 1966.
- [40] J. Srinivasan, T.E. Cheatham, P. Cieplak, P.A. Kollman, D.A. Case, *J. Am. Chem. Soc.* 120 (1998) 9401–9409.
- [41] M.B. Kroeger Smith, M.L. Lamb, J. Tirado-Rives, W.L. Jorgensen, C.J. Michejda, S.K. Ruby, R.H. Smith Jr., *Protein Eng.* 13 (2000) 413–421.
- [42] J. Wang, P. Morin, W. Wang, P.A. Kollman, *J. Am. Chem. Soc.* 123 (2001) 5221–5230.
- [43] V. Peyrot, D. Leynardier, M. Sarrazin, C. Briand, M. Menendez, J. Laynez, J.M. Andreu, *Biochemistry* 31 (1992) 11125–11132.
- [44] D.Y. Kim, K.-H. Kim, N.D. Kim, K.Y. Lee, C.K. Han, J.H. Yoon, S.K. Moon, S.S. Lee, B.L. Seong, *J. Med. Chem.* 49 (2006) 5664–5670.
- [45] For recent applications of our computational protocol see, for instance; (a) D. Zampieri, M.G. Mamolo, E. Laurini, M. Fermeglia, P. Posocco, S. Prici, E. Banfi, G. Scialino, L. Vio, *Bioorg. Med. Chem.* 17 (2009) 4693–4707; (b) M. Mazzei, E. Nieddu, M. Miele, A. Balbi, M. Ferrone, M. Fermeglia, M.T. Mazzei, S. Prici, P. La Colla, F. Marongiu, C. Ibba, R. Loddo, *Bioorg. Med. Chem.* 16 (2008) 2591–2605; (c) D. Zampieri, M.G. Mamolo, L. Vio, E. Banfi, G. Scialino, *Fermeglia, M., M. Ferrone, S. Prici, Bioorg. Med. Chem.* 15 (2007) 7444–7458 (and references therein).
- [46] A. Carta, M. Loriga, G. Paglietti, M. Ferrone, M. Fermeglia, S. Prici, T. Sanna, C. Ibba, P. La Colla, R. Loddo, *Bioorg. Med. Chem.* 15 (2007) 1914–1927.
- [47] S. Manfredini, N. Solaroli, A. Angusti, F. Nalin, E. Durini, S. Vertuani, S. Prici, M. Ferrone, S. Spadari, F. Fochar, A. Verri, E. De Clercq, J. Balzarini, *Antivir. Chem. Chemother.* 14 (2003) 183–194.
- [48] R.B. Ravelli, B. Gigant, P.A. Curmi, I. Jourdain, S. Lachkar, A. Sobel, M. Knossow, *Nature* 428 (2004) 198–202.
- [49] G. Giliberti, C. Ibba, E. Marongiu, R. Loddo, M. Tonelli, V. Boido, E. Laurini, P. Posocco, F. Fermeglia, S. Prici, *Bioorg. Med. Chem.* 18 (2010) 6055–6068.
- [50] R. Pauwels, J. Balzarini, M. Baba, R. Snoeck, D. Schols, P. Herdewijn, J. Desmyster, E. De Clercq, *J. Virol. Methods* 20 (1998) 309–321.
- [51] G.M. Morris, D.S. Goodsell, R.S. Halliday, R. Huey, W.E. Hart, R.K. Belew, A.J. Olson, *J. Comput. Chem.* 19 (1998) 1639–1662.
- [52] D.A. Case, T.A. Darden, T.E. Cheatham III, C.L. Simmerling, J. Wang, R.E. Duke, R. Luo, K.M. Merz, D.A. Pearlman, M. Crowley, R.C. Walker, W. Zhang, B. Wang, S. Hayik, A. Roitberg, G. Seabra, K.F. Wong, F. Paesani, X. Wu, S. Brozell, V. Tsui, H. Gohlke, L. Yang, C. Tan, J. Mongan, V. Hornak, G. Cui, P. Beroza, D.H. Mathews, C. Schafmeister, W.S. Ross, P.A. Kollman, *AMBER 9*. University of California, San Francisco, CA, USA, 2006.
- [53] (a) Chimera (v.1.4), Resource for Biocomputing, Visualization, and Informatics at the University of California, San Francisco (CA), USA.
(b) E.F. Pettersen, T.D. Goddard, C.C. Huang, G.S. Couch, D.M. Greenblatt, E.C. Meng, T.E. Ferrin, *J. Comput. Chem.* 25 (2004) 1605–1612.
- [54] E. Laurini, D. Zampieri, M.G. Mamolo, L. Vio, C. Zanette, C. Florio, P. Posocco, M. Fermeglia, S. Prici, *Bioorg. Med. Chem. Lett.* 20 (2010) 2954–2957.
- [55] D. Zampieri, M.G. Mamolo, E. Laurini, C. Florio, C. Zanette, M. Fermeglia, P. Posocco, M.S. Paneni, S. Prici, L. Vio, *J. Med. Chem.* 52 (2009) 5380–5392.
- [56] M. Tonelli, V. Boido, C. Canu, A. Sparatore, F. Sparatore, M.S. Paneni, M. Fermeglia, S. Prici, P. La Colla, L. Casula, C. Ibba, D. Collu, R. Loddo, *Bioorg. Med. Chem.* 16 (2008) 8447–8466.
- [57] R. Di Santo, M. Fermeglia, M. Ferrone, M.S. Paneni, R. Costi, M. Artico, A. Roux, M. Gabriele, K.D. Tardif, A. Siddiqui, S. Prici, *J. Med. Chem.* 48 (2005) 6304–6314.
- [58] B.R. Brooks, R.E. Bruccoleri, B.D. Olafson, D.J. States, S. Swaminathan, M.J. Karplus, *J. Comput. Chem.* 4 (1983) 187–217.
- [59] A. Smellie, S.L. Teig, P. Towbin, *J. Comput. Chem.* 16 (1994) 171–187.
- [60] A. Smellie, S.D. Kahn, S.L. Teig, *J. Chem. Inf. Comput. Sci.* 35 (1995) 285–294.
- [61] A. Smellie, S.D. Kahn, S.L. Teig, *J. Chem. Inf. Comput. Sci.* 35 (1995) 295–304.
- [62] A. Carta, G. Loriga, S. Piras, G. Paglietti, M. Ferrone, M. Fermeglia, S. Prici, P. La Colla, B. Secci, G. Collu, R. Loddo, *Med. Chem.* 2 (2006) 577–589.
- [63] A. Sali, T.L. Blundell, *J. Mol. Biol.* 234 (1993) 779–815.
- [64] A. Sali, L. Potterton, F. Yuan, H. van Vlijmen, M. Karplus, *Proteins* 23 (1995) 318–326.
- [65] Y. Duan, C. Wu, S. Chowdhury, M.C. Lee, G. Xiong, W. Zhang, R. Yang, P. Cieplak, R. Luo, T. Lee, J. Comput. Chem. 24 (2003) 1999–2012.
- [66] M.C. Lee, Y. Duan, *Proteins* 55 (2004) 620–634.
- [67] J. Wang, P. Cieplak, P.A. Kollman, *J. Comput. Chem.* 21 (2000) 1049–1074.
- [68] R.A. Laskowski, M.W. MacArthur, D.S. Moss, J.M. Thornton, *J. Appl. Crystallogr.* 26 (1993) 283–291.
- [69] R. Rodriguez, G. China, N. Lopez, T. Pons, G. Vriend, *CABIOS* 14 (1998) 523–528.
- [70] For the application of the MDSA protocol to different bio(macro)molecular systems, see for instance the selected list of recent publications and references therein: (a) D. Zampieri, M.G. Mamolo, L. Vio, E. Banfi, G. Scialino, M. Fermeglia, M. Ferrone, S. Prici, *Bioorg. Med. Chem.* 15 (2007) 7444–7458; (b) R. Toth, M. Ferrone, S. Miertus, E. Chiellini, M. Fermeglia, S. Prici, *Bio-macromolecules* 7 (2006) 1714–1719.
(c) E. Banfi, G. Scialino, D. Zampieri, M.G. Mamolo, L. Vio, M. Ferrone, M. Fermeglia, M.S. Paneni, S.J. Prici, *Antimicrob. Agents Chemother.* 58 (2006) 76–84.
- [71] C.I. Bayly, P. Cieplak, W.D. Cornell, P.A. Kollman, C.I. Bayly, P. Cieplak, W.D. Cornell, P.A. Kollman, *J. Phys. Chem.* 97 (1993) 10269–10280.
- [72] U.C. Singh, P.A. Kollman, *J. Comput. Chem.* 5 (1984) 129–145.
- [73] B.H. Besler, K.M. Merz, P.A. Kollman, *J. Comput. Chem.* 11 (1990) 431–439.
- [74] For a further list of recent applications of the MM/PBSA methodology from our group see, for instance: (a) M. Tonelli, I. Vazzana, B. Tasso, V. Boido, F. Sparatore, M. Fermeglia, M.S. Paneni, P. Posocco, S. Prici, P. La Colla, C. Ibba, B. Secci, G. Collu, R. Loddo, *Bioorg. Med. Chem.* 17 (2009) 4425–4440; (b) J.C. McAuliffe, W.L. Wang, G.M. Pavan, S. Prici, D. Yang, S.S. Chen, A.J. Lazar, R.E. Pollock, *J. C. Trent, Mol. Oncol.* 2 (2008) 161–163; (c) T. Negri, G.M. Pavan, E. Virdis, A. Greco, M. Fermeglia, M. Sandri, S. Prici, M.A. Pierotti, S. Pilotti, E. Tamborini, *J. Natl. Cancer Inst.* 101 (2009) 194–204; (d) M. Ferrone, F. Perrone, E. Tamborini, M.S. Paneni, M. Fermeglia, S. Suardi, E. Pastore, D. Delia, M.A. Pierotti, S. Prici, S. Pilotti, *Mol. Cancer Ther.* 5 (2006) 1467–1473; (e) E. Tamborini, S. Prici, T. Negri, M.S. Lagonigro, F. Miselli, A. Greco, A. Gronchi, P.G. Casali, M. Ferrone, M. Fermeglia, A. Carbone, M.A. Pierotti, S. Pilotti, *Oncogene* 25 (2006) 6140–6146; (f) S. Prici, M. Fermeglia, M. Ferrone, E. Tamborini, *Mol. Cancer Ther.* 4 (2005) 1167–1174; (g) M.G. Mamolo, D. Zampieri, L. Vio, M. Fermeglia, M. Ferrone, S. Prici, G. Scialino, E. Banfi, *Bioorg. Med. Chem.* 13 (2005) 3797–3809.
- [75] E.L. Mehler, T. Solmajer, *Protein Eng.* 4 (1991) 903–910.
- [76] A. Onufriev, D. Bashford, D.A. Case, *J. Phys. Chem. B.* 104 (2000) 3712–3720.
- [77] M. Feig, A. Onufriev, M. Lee, W. Im, D.A. Case, C.L. Brooks III, *J. Comput. Chem.* 25 (2004) 265–284.
- [78] F. Felluga, G. Pitacco, E. Valentini, A. Coslanich, M. Fermeglia, M. Ferrone, S. Prici, *Tetrahedron: Asymmetry* 14 (2003) 3385–3399.
- [79] V. Freccer, M. Kabelac, P. De Nardi, S. Prici, S.J. Miertus, *Mol. Graph. Model* 22 (2004) 209–220.
- [80] W.L. Jorgensen, J. Chandrasekhar, J.D. Madura, R.W. Impey, M.L. Klein, *J. Chem. Phys.* 79 (1983) 926–935.

- [81] H.J.C. Berendsen, J.P.M. Postma, W.F. Van Gunsteren, A. DiNola, J.R. Haak, *J. Chem. Phys.* 81 (1984) 3684–3690.
- [82] J.P. Ryckaert, G. Ciccotti, H.J.C. Berendsen, *J. Comput. Phys.* 23 (1977) 327–341.
- [83] A. Toukmaji, C. Sagui, J. Board, T. Darden, *J. Chem. Phys.* 113 (2000) 10913–10927.
- [84] P.A. Kollman, I. Massova, C. Reyes, B. Kuhn, S. Huo, L. Chong, M. Lee, T. Lee, Y. Duan, W. Wang, O. Donini, P. Cieplak, J. Srinivasan, D. Case, T.E. Cheatham III, *Acc. Chem. Res.* 3 (2000) 889–897.
- [85] M.K. Gilson, K.A. Sharp, B.H. Honig, Calculating the electrostatic potential of molecules in solution – method and error assessment, *J. Comput. Chem.* 9 (1988) 327–335.
- [86] D. Sitkoff, K.A. Sharp, B.H. Honig, *J. Phys. Chem.* 98 (1994) 1978–1988.
- [87] M.F. Sanner, A.J. Olson, J.C. Spehner, *Biopolymers* 38 (1996) 305–320.
- [88] E.B. Wilson, J.C. Decius, P.C. Cross, *Molecular Vibrations*. McGraw-Hill, New York, NY, 1995.